Rock Mechanics and Rock Engineering (2022) 55:2747–2769
https://doi.org/10.1007/s00603-021-02628-3

ORIGINAL PAPER

Generalized Block Theory for the Stability Analysis of Blocky Rock Mass Systems Under Seismic Loads

Shuaifeng Wang[1,2] · Zixin Zhang[1,2] · Xin Huang[1,2] · Qinghua Lei[3]

Received: 7 January 2021 / Accepted: 19 August 2021 / Published online: 9 September 2021

Abstract

The stability analysis of rock blocks on man-made excavation faces (e.g. tunnel, cavern, and slope) subject to seismic loads is an important issue in the field of rock engineering. This paper proposes a generalized block theory (GBT) by combining a pseudo-static method and the traditional block theory to evaluate the stability of blocky rock masses during earthquake activities. In our analysis, the basic safety factors are derived considering time-varying seismic loads to determine the stability of a rock block at each time step. Afterwards, two new parameters, P^u and V^u, are used to evaluate the seismic stability of a rock block, where P^u is the instability probability defined as the ratio of the time for the block becoming unstable to the total seismic loading time, and V^u is the probabilistic instability volume defined as P^u times the block volume. As for a blocky rock mass system, its probabilistic instability volume is the sum of V^u of all seismically unstable blocks and the instability probability is the ratio of its probabilistic instability volume and total volume of seismically unstable blocks. Through the simulation of a generic slope excavation, we observe that seismic loads significantly affect the stability and kinematics of a rock block during an earthquake. For a blocky rock mass, both P^u and V^u decay with the epicentral distance, in general following an inverse power law trend. Furthermore, it is found that the local site effect also has a strong influence on the slope stability under seismic loads.

Keywords Blocky rock mass · Generalized block theory · Seismic loads · Evaluation parameter

List of Symbols

a_1^t, a_2^t	Accelerations along two orthogonal directions on the horizontal plane
a_x^t, a_y^t, a_z^t	Seismic accelerations in the directions of east–west, north–south and vertical, respectively
A_i	Area of the contacting surface of the block on joint i
card()	Counting function for a set
c_i	Cohesion of joint i
$\mathbf{D}$	Determination matrix
D_k^{ij}	A representative element of determination matrix $\mathbf{D}$
$f^{0,t}$	Safety factor for free translation
$f^{1,t}$	Safety factor for single-plane sliding
$f^{2,t}$	Safety factor for double-plane sliding
$\mathbf{F}^{a,t}$	Active force at time t
$\mathbf{F}^{d,t}$	Driving force at time t
$F^{d,t}$	Modulus of $\mathbf{F}^{d,t}$
$\mathbf{F}^{r,t}$	Tangential resistance force at time t
$F^{r,t}$	Modulus of $\mathbf{F}^{r,t}$
$\mathbf{F}^S$	Force induced by the in-situ stress
$\mathbf{F}^{s,t}$	The seismic loads at time t
$\mathbf{F}^W$	Water pressure
$\mathbf{G}$	Self-gravity of a rock block
φ_i	Friction angle of joint i
m	Mass of a rock block
$\mathbf{M}^T$	Coordinate transformation matrix
M_{w}	Moment magnitude of an earthquake
$\mathbf{n}^{a,t}$	Unit vector of the resultant active force $\mathbf{F}^{a,t}$ at time t
$\mathbf{n}_i$	Upward unit normal vector of joint i
$\mathbf{N}^t$	Normal reaction force at time t

✉ Zixin Zhang
zxzhang@tongji.edu.cn

[1] Department of Geotechnical Engineering, College of Civil Engineering, Tongji University, No. 1239 Siping Road, Yangpu District, Shanghai 200092, People's Republic of China

[2] Key Laboratory of Geotechnical and Underground Engineering, Ministry of Education, Tongji University, Shanghai, People's Republic of China

[3] Department of Earth Sciences, ETH Zürich, Zürich, Switzerland

$\mathbf{N}_i^t$	Normal reaction force along joint i at time t
N_i^t	Normal reaction force along joint i at time t, modulus of $\mathbf{N}_i^t$
N_j^t	Normal reaction force along joint j at time t
P^u	Instability probability of a blocky rock mass system
P_i^u	Instability probability of a block number i under time-varying active forces
R_{epi}	Epicentral distance, i.e. the distance of a site or a seismic station from the epicenter
S_l^D	A set storing joint pairs along which double-plane sliding happens
S^D	A set storing joints along which single-plane sliding happens
$\mathbf{s}^t$	Sliding direction at time step t
$\mathbf{s}_i^t$	Sliding direction along joint i at time t
$\mathbf{s}_j^t$	Sliding direction along joint j at time t
$\mathbf{s}_{ij}^t$	Sliding direction along joints i and j at time t
sign()	Sign function
θ	The angle counterclockwise from a_1^t to east–west direction
T^{unstable}	Duration time when the block is unstable
T^{total}	Total seismic loading time
$\mathbf{v}_i$	Normal unit vector of joint plane i, directing into the rock block
$\mathbf{v}_j$	Normal unit vector of joint plane j, directing into the rock block
$\mathbf{v}_k$	Normal unit vector of joint plane k, directing into the rock block
V^u	Probabilistic instability volume of a blocky rock mass system
V_i^u	Probabilistic instability volume of a block number i under time-varying active forces

1 Introduction

Rock masses in nature can be generally categorized into relatively intact rock masses, blocky rock masses, and heavily fractured rock masses according to the density of discontinuities (Hoek 1983; Hoek and Brown 1997). Different numerical methods have been developed over the past years to deal with different types of rock masses. Specifically developed for blocky rock masses, block theory (Goodman and Shi 1985), discrete element method (Cundall 1988), and discontinuous deformation analysis (Shi 1988) are the most commonly used approaches for numerical simulation to assess surrounding rock stability in geoengineering applications. The block theory, which was originally proposed by Goodman and Shi (1985), is an efficient and effective method for analyzing the influence of discontinuities on the stability of rock blocks subject to artificial excavations. The applicability and effectiveness of the original block theory has been well demonstrated by various engineering-related studies in the past decade, including block identification and visualization (Yu et al. 2009; Zhang and Lei 2014; Zheng et al. 2015b, 2019; Zhang et al. 2017b), removability analysis of rock blocks (Li et al. 2012; Wu et al. 2017; Wang et al. 2021), stability analysis of rock blocks (Kulatilake et al. 2011; Zhang and Lei 2013; Wu et al. 2015; Zheng et al. 2016; Zhang et al. 2018, 2019; Tonon 2020), probability analysis of unstable blocks (Zheng et al. 2014; Zheng et al. 2015a; Jia et al. 2017), key-block group analysis (Noroozi et al. 2012; Fu and Ma 2014) and support design (Prasad et al. 2013; Fu and Ma 2014; Zhang et al. 2014, 2020; Wu et al. 2015; Liu et al. 2017). These past studies were mainly based on the static calculations and thus focused on the stability of rock blocks under static loads, which cannot deal with the stability of rock blocks under seismic loads during e.g. earthquake activities.

Due to frequently occurring natural/anthropogenic earthquakes worldwide, rock engineering often needs to deal with seismic effects. The traditional block theory is capable of dealing with rock engineering problems without seismic loads since only the static limit-equilibrium equation is considered. The self-gravity of a block is constant while the seismic loads during an earthquake change over time, leading to a time-dependent dynamic force. Consequently, it is highly likely that the stability of a rock block may alter in the presence of time-varying seismic loads. When considering the seismic loads induced by earthquakes, there are two approaches to analyze the stability of rock blocks in the context of block theory: the pseudo-static method (Terzaghi et al. 1996; Zhang 2018; Rocscience UnWedge 2020) and the Newmark method (Newmark 1965; Bakun-Mazor et al. 2012; Zhang 2018; Fu et al. 2019). The pseudo-static method is inherently simple in computation, in which the earthquake effect is treated in an equivalent way as time-sequential static loads imposed at the centroid of a rock block (Rocscience SWedge 2020). Here, the Rocscience platform assesses the effect of seismic loads on block stability by re-running the analysis procedures with several different directions for the seismic forces (Rocscience SWedge 2020; Rocscience UnWedge 2020), which may be computationally expensive when considering seismic load time series consisting of a large number of signals. The Newmark method treats the seismic loads as dynamic inertial forces changing with time and calculates the accelerations by solving the mechanical equilibrium equation with the displacement derived through double integration of acceleration in each time step (Ghosh and Haupt 1989; Law and Lam 2003; Jibson 2011; Bakun-Mazor et al. 2012; Roy et al. 2016; Fu et al. 2019). As a result, the Newmark method needs to calculate the trial of the incremental displacement and subsequently check the block contact in each time step (Fu et al. 2019), which may

be computationally inefficient. In addition, most of the previous studies using the block theory to assess the stability of a rock block under seismic loads mainly focused on the scenario of a single block, whereas the stability of a blocky rock mass system has not been well explored.

This paper proposes a generalized block theory (GBT) combining the pseudo-static method and the traditional block theory to investigate the stability of blocky rock masses subject to earthquakes. We elaborate the proposed method including the basic assumptions, the generation of a blocky rock mass system, the removability and kinematics analysis of rock blocks, and the formulation for seismic stability analysis. The stability of a blocky rock mass under an earthquake is quantified by two parameters: instability probability value and probabilistic instability volume. This new method is implemented in our in-house code BLKLAB (Zhang and Lei 2013). Finally, the applicability and effectiveness of our method are demonstrated by studying a generic rock engineering problem, where the influences of earthquake magnitude, epicentral distance and local site effect are investigated.

2 Generalized Block Theory for Stability Analysis Under Seismic Loads

The GBT combines the traditional block theory and the pseudo-static method to assess the stability of blocky rock masses under seismic loads during earthquake events.

2.1 Basic Assumptions

The GBT follows the basic assumptions of the traditional block theory (Goodman and Shi 1985), including planar joints, rigid blocks and polygonal joint shape. The joint of a disc shape is assumed to have an arbitrary radius, such that a joint with an infinite radius extends entirely across the domain of interest while a finite-sized joint may terminate inside the domain. Furthermore, the kinematic modes are limited to free translation (separation from host rock), single-plane sliding or double-plane sliding. Sliding corresponds to shear failure along the joint surface obeying the Mohr–Coulomb failure criterion controlled by the cohesion and friction angle of the joint.

The self-gravity of a block is a stationary body force, while the seismic loads caused by earthquakes are time-dependent. According to the pseudo-static method, the time series of a varying force are assumed to be degenerated as a discrete series of forces at different time steps. Thus, the time-sequential seismic loads are regarded as external forces exerted at the barycenter of a rock block at each time step. In the context of the pseudo-static method, the GBT gives an approximate solution to the transient process during a time step without directly solving the inertia term as well as accumulated velocity and displacement.

The GBT mainly consists of three steps: (1) generation of a geometrical model for a blocky rock mass system, (2) identification of geometrical removability and kinematic modes of rock blocks, and (3) determination of mechanical stability of removable rock blocks under seismic loads. The last procedure is pivotal for the GBT.

2.2 Generation of Geometrical Model for Blocky Rock Mass Systems

The first step to study the behavior of rock blocks is to generate a geometrical model for blocky rock masses. The paper utilizes a block cutting and assembling algorithm to generate rock blocks, which was originally proposed by Zhang and Lei (2013) and subsequently improved by Zhang et al. (2017a, b). The main procedures of block cutting and assembling are illustrated in Fig. 1 and described as follows: (a) generate a finite computational domain embedded with joints according to geometrical input data (Fig. 1a); (b) temporarily assume joints are infinite and use them to split the computational domain into element blocks of convex shapes (E1–E8 in Fig. 1b); (c) consider the actual sizes and shapes of joints and merge them to form complex blocks of either convex or concave shapes (C1–C3 in Fig. 1c); (d) generate the excavation surfaces for considering an artificial excavation (excavation in Fig. 1d); (e) detect the element blocks influenced by the excavation surfaces (Fig. 1e) and cut them using the excavation surfaces (Fig. 1f); (f) remove the element blocks located inside the excavation space (Fig. 1g) and re-assemble the remaining element blocks into complex blocks (Fig. 1h). After the re-assembly of complex blocks in the last procedure, the joint blocks (only formed by joints, JC1 in Fig. 1h) and excavated blocks (formed by joints and excavation surfaces, EC2 and EC3 in Fig. 1h) are generated. It is clear that only excavated blocks will potentially be key blocks that may become unstable first and thus control the stability of other secondary blocks (e.g. some of the joint blocks adjacent to the excavation). The following analysis of geometrical removability and mechanical stability are focused on excavated blocks.

2.3 Geometrical Removability and Kinematics

In this paper, an improved stereo-analytical method, which is based on the original stereo-analytical method (Zhang and Kulatilake 2003) and the generalized joint pyramid method (Wang et al. 2021), is employed to analyze the removability of rock blocks. Compared to conventional approaches, the removability analysis procedure is improved in the following two aspects. First, the joint planes have the ability to restrict the movement of blocks,

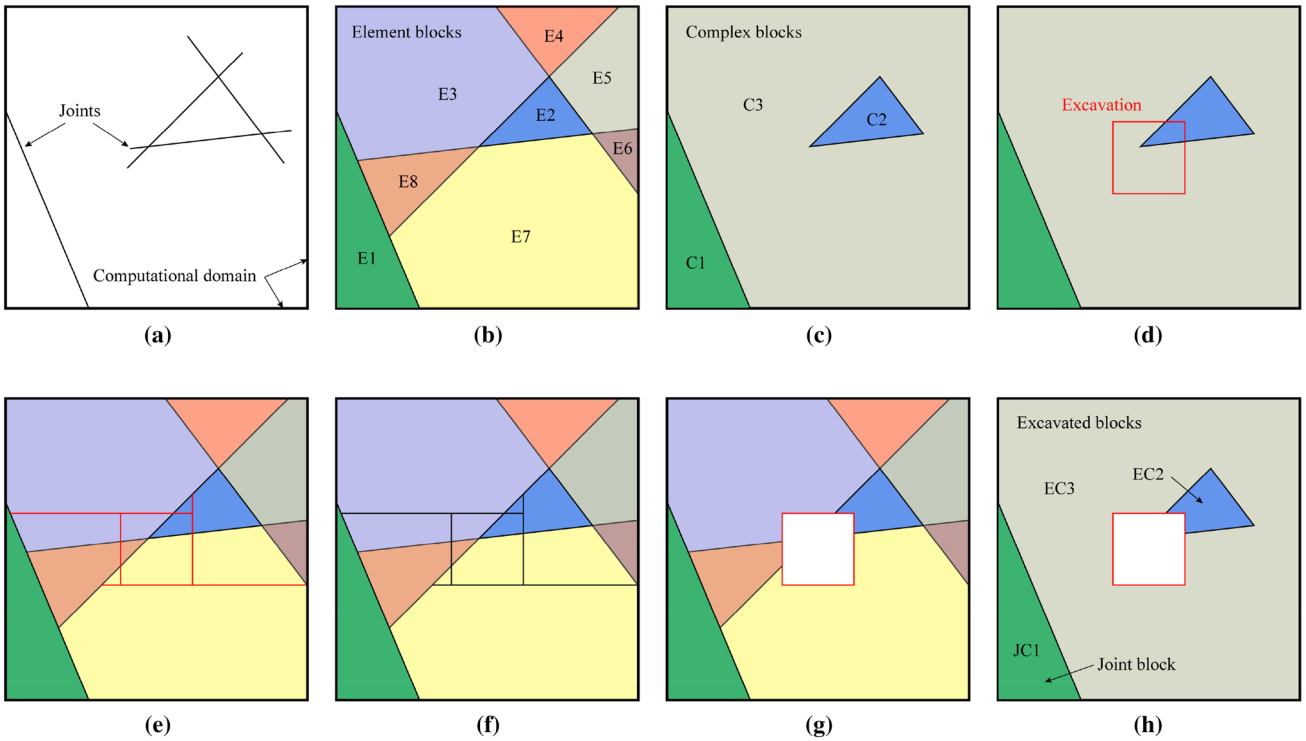

Fig. 1 Procedures of geometrical model generation: **a** generate computational domain and joints; **b** split the rock system into element block ignoring the joints' extension; **c** assembly element blocks into groups considering the actual size of joints and merge them into complex blocks; **d** generate artificial excavation surfaces; **e** detect influenced block by excavation; **f** cut the influenced element blocks using excavation surfaces; **g** remove the element blocks located in the excavation space; **h** re-merge complex blocks after excavation

but the excavation surfaces make no contribution to the block's motion. Subject to the finiteness of blocks in the geometrical model, the block pyramid is inherently empty, which can be ignored in the analysis. Thus, only joints forming the block should be taken into account when identifying its removability. Second, a finite block is removable only when all the points belonging to the block are removable due to the assumption of rigid-body translation. The removability of a block is the intersection of the removability of the points, which is independent of the geometrical convexity. Therefore, it is not necessary to divide a concave block into convex sub-blocks to indirectly identify the removability of the concave block based on the removability of its sub-blocks. Thus, a generalized joint pyramid (GJP) is defined as the intersection of half-spaces of all the joints forming the block, neglecting the excavation surfaces and the block's concavity. The removability theorem for a rock block can then be simplified as: a given finite block B (convex or concave) is removable if its GJP is non-empty.

The improved stereo-analytical method uses the determination matrix $\mathbf{D}$ to identify the emptiness of a rock block's GJP and then examine its removability. $\mathbf{D}$ is a matrix consisting of -1, 0 and 1 with dimension $C_n^2 \times n$, where n is the number of joints forming the rock block, expressed as:

$$\mathbf{D} = \left[D_k^{ij}\right]_{C_n^2 \times n} = \begin{array}{c} \begin{matrix} k \rightarrow & 1 & 2 & 3 & \ldots & n \end{matrix} \\ \begin{bmatrix} 0 & 0 & 1 & \ldots & 1 \\ 0 & -1 & 0 & \ldots & -1 \\ \ldots & \ldots & \ldots & \ldots & \ldots \\ 0 & -1 & -1 & \ldots & 0 \\ 1 & 0 & 0 & \ldots & -1 \\ 1 & 0 & -1 & \ldots & -1 \\ \ldots & \ldots & \ldots & \ldots & \ldots \\ -1 & 0 & -1 & \ldots & 0 \\ \ldots & \ldots & \ldots & \ldots & \ldots \\ -1 & -1 & 1 & \ldots & 0 \end{bmatrix} \end{array} \begin{array}{cc} i & j \\ \downarrow & \downarrow \\ 1 & 2 \\ 1 & 3 \\ \ldots & \ldots \\ 1 & n \\ 2 & 3 \\ 2 & 4 \\ \ldots & \ldots \\ 2 & n \\ \ldots & \ldots \\ n-1 & n \end{array} \tag{1}$$

where D_k^{ij} is a representative element of $\mathbf{D}$. The detailed theoretical derivation of the GJP method and determination matrix $\mathbf{D}$ can be found in Wang et al. (2021). The analysis procedures for a rock block's removability are briefly summarized as below:

Step 1: Loop all the rows of $\mathbf{D}$ and go to step 2.
Step 2: If the lth row D_k^{ij} of $\mathbf{D}$ is a mixture of -1 and 0 or + 1 and 0, create a sub-set to store indexes i and j, denoted as $S_l^D = \{i, j\}$ for $l \in \left\{1, 2, ..., C_n^2\right\}$; let $S_l^D = \emptyset$ if the row is a mixture of -1, 0 and + 1.

Step 3: After the loop, create a union-set to store all the existing elements of the above sub-sets, denoted as $S^D = \bigcup_{l=1}^{C_n^2} S_l^D$.

Step 4: Identification of removability. If $S^D \neq \emptyset$, the corresponding GJP is non-empty and the corresponding block is removable; if $S^D = \emptyset$, the GJP is empty and the block is non-removable (also called tapered).

Step 5: Determination of kinematic modes. Single-plane sliding happens to joints with indexes in S^D and double-plane sliding occurs on joint pairs with indexes in the non-empty S_l^D.

2.4 Stability Analysis of Blocky Rock Mass Systems Under Seismic Loads

In this part, the mechanical stability analysis of rock blocks under seismic loads is only focused on the removable blocks.

2.4.1 Determination of Seismic Loads

The ground motion under earthquakes is a nonstationary random process, which can be recorded by seismic monitoring stations (Mousavi and Beroza 2020). As a result, the induced seismic accelerations vary over time during an earthquake, which are represented by the accelerograms marching with time. Usually, the monitoring station records the accelerations in three orthogonal directions, e.g. the north–south, east–west and vertical directions, as shown in Fig. 2. The seismic load $\mathbf{F}^{s,t}$ at time t is given as

$$\mathbf{F}^{s,t} = m \cdot \mathbf{a}^t = m \cdot \left(a_x^t, a_y^t, a_z^t\right), \tag{2}$$

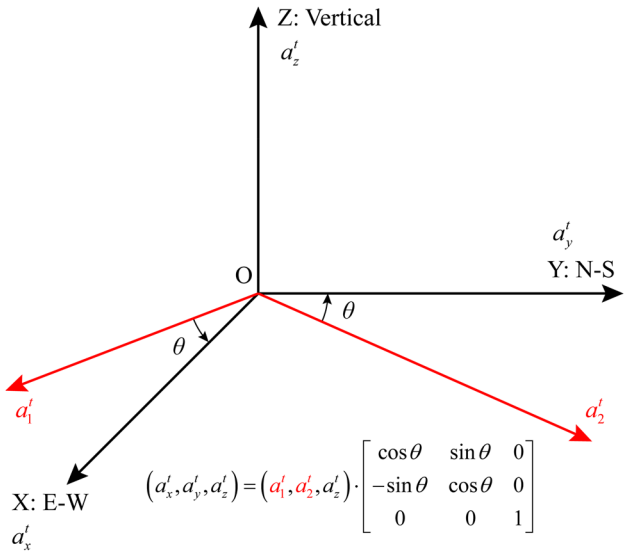

Fig. 2 Seismic accelerations in the 3D space

where m is the mass of a rock block; $\mathbf{a}^t$ is a vector denoting the acceleration at time t; a_x^t, a_y^t and a_z^t are the seismic accelerations in the directions of east–west, north–south and upright, respectively. Sometimes, the monitoring station records the horizontal accelerations a_1^t and a_2^t in directions with a certain angle relative to the east–west and north–south directions (Fig. 2). For example, the Yarimca Petkim station recorded horizontal accelerations of Kocaeli earthquake in the directions of NE60° and NW30° (Yenier et al. 2010; Giardini et al. 2013). For such cases, the acceleration vector $\left(a_1^t, a_2^t, a_z^t\right)$ can be transformed into the standard east–west and north–south directions using the following equation

$$\left(a_x^t, a_y^t, a_z^t\right) = \left(a_1^t, a_2^t, a_z^t\right) \cdot \mathbf{M}^T = \left(a_1^t, a_2^t, a_z^t\right) \cdot \begin{bmatrix} \cos\theta & \sin\theta & 0 \\ -\sin\theta & \cos\theta & 0 \\ 0 & 0 & 1 \end{bmatrix}, \tag{3}$$

where $\mathbf{M}^T$ is the transformation matrix and θ is the angle counterclockwise from a_1^t to east–west (also from a_2^t to north–south) as shown in Fig. 2.

2.4.2 Safety Factor of a Single Rock Block Under Seismic Loads

For a removable block B, its mechanical condition is schematically illustrated in Fig. 3. Forces acting on a given block B include three components: (1) an active force $\mathbf{F}^{a,t}$, compounded by block gravity and other external forces; (2) a normal reaction force $\mathbf{N}^t$, which is normal to the sliding direction; (3) a tangential resistance force $\mathbf{F}^{r,t}$, which is parallel to the sliding direction. The active force $\mathbf{F}^{a,t}$ will induce a driving force $\mathbf{F}^{d,t}$ urging the block to slide along a certain direction while the movement is resisted by the tangential resistance force $\mathbf{F}^{r,t}$. The final stability status of the block is determined by the ratio of $\mathbf{F}^{r,t}$ to $\mathbf{F}^{d,t}$, which is usually called safety factor. The superscript t in subsequent formulae denotes a representative time t to emphasize that the forces are temporally varying. Formulae without superscript t in the following text denote

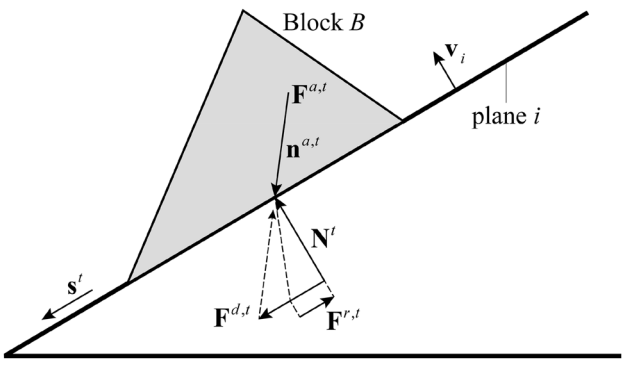

Fig. 3 Schematic of forces acting on a removable block (modified from Goodman and Shi 1985)

constants that are invariant over time. For a block in the rock mass system, the resultant active force can be generally written as

$$\mathbf{F}^{a,t} = \mathbf{G} + \mathbf{F}^{W} + \mathbf{F}^{S} + \mathbf{F}^{s,t}, \tag{4}$$

where $\mathbf{F}^{a,t}$ is the resultant active force at time t; $\mathbf{G}$ is the self-gravity of a rock block; $\mathbf{F}^{W}$ is the water pressure; $\mathbf{F}^{S}$ is the force induced by the in situ stress; $\mathbf{F}^{s,t}$ is the seismic loads at time t.

In the presence of unbalanced forces, the GBT investigates three kinds of translational modes: free translation (departure from the host rock), single-plane sliding and double-plane sliding. The basic factors of safety for the three types of movements are derived as follows.

Free translation corresponds to a detachment of the block from the host rock. In such a case, there is no reaction force from joints. Therefore, the movement direction at time t is the same as that of the resultant active force, derived as

$$\mathbf{s}^{t} = \mathbf{n}^{a,t} = \frac{\mathbf{F}^{a,t}}{|\mathbf{F}^{a,t}|}, \tag{5}$$

where $\mathbf{s}^{t}$ is the block moving direction at time step t; $\mathbf{n}^{a,t}$ is the unit vector of the resultant active force $\mathbf{F}^{a,t}$ at time t. In this case, all the surfaces of the block depart from the host rock under the active force. The sufficient and necessary condition for a block to undergo free translation is expressed as:

$$\mathbf{s}^{t} \cdot \mathbf{v}_{i} \geq 0, \tag{6}$$

where $\mathbf{v}_{i}$ is the normal unit vector of joint plane i, directing into the block. The resistance force is 0 due to the absence of the reaction forces from joints. Thus, the safety factor for free translation is 0, i.e.,

$$f^{0,t} = 0. \tag{7}$$

As for single-plane sliding, the reaction force comes from one single joint that controls the block motion. The sliding direction can be derived by the orthogonal projection of $\mathbf{n}^{a,t}$ on joint i, expressed as

$$\mathbf{s}^{t} = \mathbf{s}_{i}^{t} = \frac{\left(\mathbf{n}_{i} \times \mathbf{n}^{a,t}\right) \times \mathbf{n}_{i}}{\left|\mathbf{n}_{i} \times \mathbf{n}^{a,t}\right|}, \tag{8}$$

where $\mathbf{n}_{i}$ is the upward unit normal vector of joint i. The relationship between $\mathbf{n}_{i}$ and $\mathbf{v}_{i}$ is: if the block is located in the upper half-space of plane i, $\mathbf{v}_{i} = \mathbf{n}_{i}$; otherwise, $\mathbf{v}_{i} = -\mathbf{n}_{i}$. The sufficient and necessary condition for the block to slide along a single plane i is

$$\begin{cases} \mathbf{v}_{i} \cdot \mathbf{n}^{a,t} \leq 0 \\ \mathbf{v}_{j} \cdot \mathbf{s}^{t} > 0, \ \text{for}(j \neq i) \end{cases}, \tag{9}$$

Under this condition, the driving force $\mathbf{F}^{d,t}$ (Fig. 3) at time t is the projection of $\mathbf{F}^{a,t}$ on the sliding direction $\mathbf{s}^{t}$ on joint i, given as

$$\mathbf{F}^{d,t} = F^{d,t} \cdot \mathbf{s}^{t} = \left|\mathbf{F}^{a,t} \cdot \mathbf{s}^{t}\right| \cdot \mathbf{s}^{t}. \tag{10}$$

The corresponding resistance force $\mathbf{F}^{r,t}$ consists of the friction and cohesion on joint i, which can be derived from the component of normal reaction force $\mathbf{N}_{i}^{t}$ induced by $\mathbf{F}^{a,t}$, along the opposite direction of sliding $\mathbf{s}^{t}$. The normal reaction force $\mathbf{N}_{i}^{t}$ and the resistance force $\mathbf{F}^{r,t}$ are expressed as:

$$\mathbf{N}_{i}^{t} = N_{i}^{t} \cdot \mathbf{n}_{i} = \left|\mathbf{F}^{a,t} \cdot \mathbf{n}_{i}\right| \cdot \mathbf{n}_{i}, \tag{11}$$

$$\mathbf{F}^{r,t} = -F^{r,t} \cdot \mathbf{s}^{t} = -\left(N_{i}^{t} \cdot \tan\varphi_{i} + A_{i} \cdot c_{i}\right) \cdot \mathbf{s}^{t}, \tag{12}$$

where φ_{i} and c_{i} are the friction angle and cohesion of joint i, respectively; A_{i} is the area of the contacting surface of the block on joint i. The safety factor $f^{1,t}$ for single-plane sliding is derived as

$$f^{1,t} = \frac{F^{r,t}}{F^{d,t}} = \frac{N_{i}^{t} \cdot \tan\varphi_{i} + A_{i} \cdot c_{i}}{|\mathbf{F}^{a,t} \cdot \mathbf{s}^{t}|}. \tag{13}$$

In the double-plane sliding mode, the block slides along the intersection line of two joint planes, numbered as i and j. The sliding direction is parallel to the intersection line and forms an acute angle with $\mathbf{F}^{a,t}$, given as

$$\mathbf{s}^{t} = \mathbf{s}_{ij}^{t} = \frac{\mathbf{n}_{i} \times \mathbf{n}_{j}}{\left|\mathbf{n}_{i} \times \mathbf{n}_{j}\right|} \text{sign}\left(\left(\mathbf{n}_{i} \times \mathbf{n}_{j}\right) \cdot \mathbf{n}^{a,t}\right), \tag{14}$$

where sign() is the sign function. The sufficient and necessary condition for the block to undergo a double-plane sliding is

$$\begin{cases} \mathbf{v}_{i} \cdot \mathbf{s}_{j}^{t} \leq 0 \\ \mathbf{v}_{j} \cdot \mathbf{s}_{i}^{t} \leq 0 \\ \mathbf{v}_{k} \cdot \mathbf{s}^{t} > 0, \ \text{for}(k \neq i,j) \end{cases}, \tag{15}$$

where $\mathbf{s}_{i}^{t}$ and $\mathbf{s}_{j}^{t}$ are the orthographic projections of $\mathbf{n}^{a,t}$ on joint planes i and j, respectively, and can be obtained by Eq. (8). The driving force $\mathbf{F}^{d,t}$ at time t is the orthogonal projection of $\mathbf{F}^{a,t}$ on the intersection line, given as

$$\mathbf{F}^{d,t} = F^{d,t} \cdot \mathbf{s}^{t} = \left|\mathbf{F}^{a,t} \cdot \mathbf{s}^{t}\right| \cdot \mathbf{s}^{t} = \frac{\left|\mathbf{F}^{a,t} \cdot \left(\mathbf{n}_{i} \times \mathbf{n}_{j}\right)\right|}{\left|\mathbf{n}_{i} \times \mathbf{n}_{j}\right|} \cdot \mathbf{s}^{t}. \tag{16}$$

The resistance forces at this time step are distributed in both two sliding planes, expressed as

$$\mathbf{F}^{r,t} = -F^{r,t} \cdot \mathbf{s}^t = -\Big(\big(N_i^t \cdot \tan\varphi_i + A_i \cdot c_i\big) + \Big(N_j^t \cdot \tan\varphi_j + A_j \cdot c_j\Big)\Big) \cdot \mathbf{s}^t, \tag{17}$$

where N_i^t and N_j^t are the normal reaction forces on joints i and j at time t, respectively:

$$N_i^t = \frac{\left|\left(\mathbf{F}^{a,t} \times \mathbf{n}_j\right) \cdot \left(\mathbf{n}_i \times \mathbf{n}_j\right)\right|}{\left|\mathbf{n}_i \times \mathbf{n}_j\right|^2}, \tag{18}$$

$$N_j^t = \frac{\left|\left(\mathbf{F}^{a,t} \times \mathbf{n}_i\right) \cdot \left(\mathbf{n}_i \times \mathbf{n}_j\right)\right|}{\left|\mathbf{n}_i \times \mathbf{n}_j\right|^2}. \tag{19}$$

Then, the safety factor for double-plane sliding is derived as

$$f^{2,t} = \frac{F^{r,t}}{F^{d,t}} = \frac{\left(N_i^t \cdot \tan\varphi_i + A_i \cdot c_i\right) + \left(N_j^t \cdot \tan\varphi_j + A_j \cdot c_j\right)}{\left|\mathbf{F}^{a,t} \cdot \mathbf{s}^t\right|}. \tag{20}$$

The block is recognized as a key block or an unstable block if the safety factor is less than a prescribed threshold, usually set as 1. Using Eqs. (7), (13) and (20), a rock block can be determined as stable or unstable at any time during the seismic loading. The calculation degenerates to the static analysis of the traditional block theory if the seismic load $\mathbf{F}^{s,t}$ is zero in Eq. (4).

2.4.3 Evaluation Parameters for Seismic Stability

Generally, the basic safety factor is capable of indicating the stability of a rock block if only considering constant forces, which is equivalent to the static analysis in the original block theory. When time-varying forces are imposed on the block, the occurrence probability for an unstable status should be computed. Herein, the instability probability for a block i under time-varying forces is defined as follows

$$P_i^u = \frac{T_i^{\text{unstable}}}{T_i^{\text{total}}} \times 100\%, \tag{21}$$

where T_i^{unstable} is the duration time when the block is unstable; T_i^{total} is the total seismic loading time. A removable block is defined as a seismically unstable block if its instability probability is larger than 0, i.e. $P_i^u > 0$. Otherwise, the removable block is identified as a seismically stable block.

In addition to the safety factor, the volume of an unstable block is usually used to represent its hazardousness in the static analysis (Wu et al. 2015). Herein, the probabilistic instability volume V_i^u of a seismically unstable block is defined as

$$V_i^u = V_i \cdot P_i^u, \tag{22}$$

where V_i and P_i^u are the volume and instability probability of block i, respectively. The seismic stability of a rock block can be represented by the afore-defined two parameters. To evaluate the seismic stability of a blocky rock mass, the total probabilistic instability volume V^u is calculated as

$$V^u = \sum_{i=1}^{q} V_i^u = \sum_{i=1}^{q} V_i \cdot P_i^u, \tag{23}$$

where q is the number of seismically unstable blocks in the rock mass. Taking the blocks' volume as weight, the instability probability of the blocky rock mass P^u is defined as

$$P^u = \frac{V^u}{\sum_{i=1}^{q} V_i} \times 100\%. \tag{24}$$

These two parameters, i.e. the probabilistic instability volume and instability probability, are used in this paper to evaluate the stability of a blocky rock mass during earthquakes.

2.5 Implementation in BLKLAB

An in-house modeling platform named block laboratory or BLKLAB was developed by Zhang and Lei (2013, 2014) using an object-oriented programming technique to implement the original block theory together with morphological visualization for the analysis of complex block systems. In recent years, BLKLAB incorporated two major updates: (1) Wu et al. (2015) improved the computational efficiency of the morphological visualization and Zhang et al. (2017b) improved the geometrical accuracy of the block cutting and assembling algorithm; (2) Zhang et al. (2017a, 2018, 2019) developed a TBM (abbreviation for tunnel boring machine) tunneling simulation module in BLKLAB, enabling the stability analysis of rock blocks during TBM tunnel constructions. In this paper, the GBT with the capability of analyzing block stability under seismic loads is implemented into BLKLAB. The modeling steps are briefly summarized as follows

Step 1: Establish an appropriate computational domain.
Step 2: Import joints data and generate an original blocky rock mass system.
Step 3: Import excavation data and generate the excavated blocky rock mass system.

Step 4: Loop all the excavated rock blocks in the system and identify removable blocks.
Step 5: Loop all the removable blocks and identify the unstable blocks under static loads.
Step 6: Import seismic acceleration data and evaluate the stability of removable blocks under seismic loads.

Although the traditional block theory has proven to be a practically useful and efficient method to deal with rock engineering in blocky rock masses (Goodman and Shi 1985; Wu et al. 2015; Liu et al. 2017; Zhang et al. 2020), it is still important to examine the validity of our new GBT method. This may be done via a comparison with another independent method. Here, we compare our GBT model with the commercial software 3DEC, which is based on the discrete element method (3DEC Manual 2019). The details of this comparison are presented in Appendix A.

3 Simulation Examples

A generic rock slope problem is studied to demonstrate the applicability and effectiveness of the GBT for the stability analysis of rock blocks under seismic loading.

3.1 Problem Statement

A rock slope of 15 m high is shown in Fig. 4: the upper region is 6.79 m high with a dip angle of 50° and the lower region is 8.21 m high with a dip angle of 35°. The dip directions of the excavation surfaces are along the y-axis. The slope length along the strike (i.e. the x-axis) is 30 m. The orientations of joint sets are listed in Table 1, referring to Goodman and Shi (1985, page 303). For joint set 4, the infinite spacing indicates that there is only one joint plane in this joint set. All the joints in the model are assumed to extend infinitely in the 3D space, i.e. their radii are infinite, as shown in Table 1. In this paper, the cohesion of joints is set as 0. The density of the rock is 2400 kg/m^3,

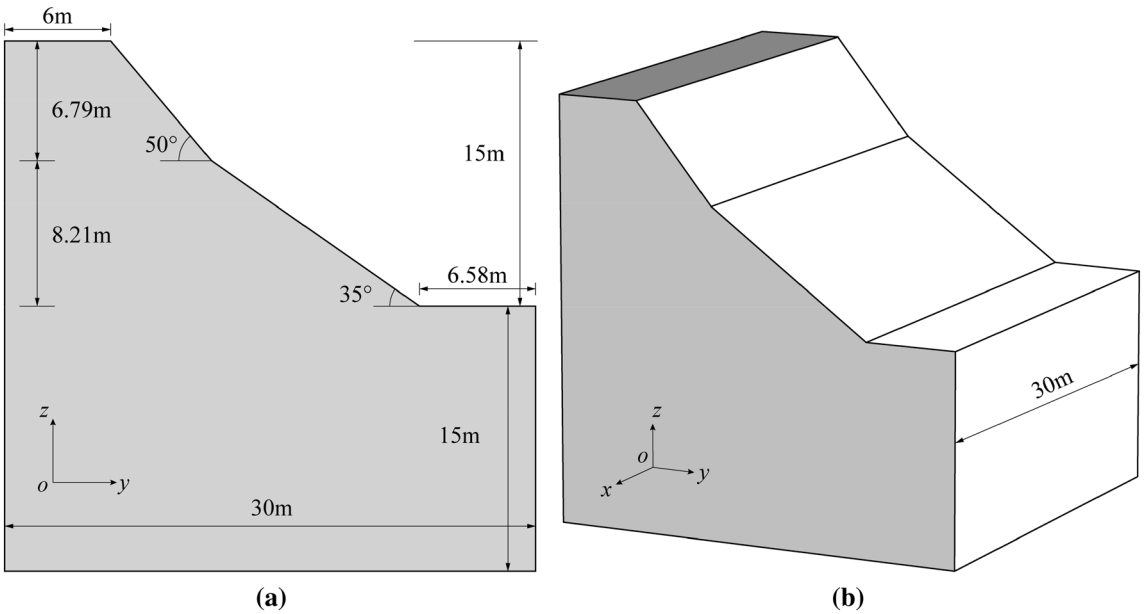

Fig. 4 Geometrical information of the slope project: **a** a side view; **b** an oblique view

Table 1 Geometrical and mechanical parameters of joint sets

Joint set ID	Dip angle (°)	Dip direction (°)	Friction angle (°)	Spacing (m)	Radius (m)	Number of joints
1	71	163	15	5	Infinite	9
2	68	243	20	5	Infinite	9
3	45	280	31	5	Infinite	9
4	13	343	16	Infinite	Infinite	1

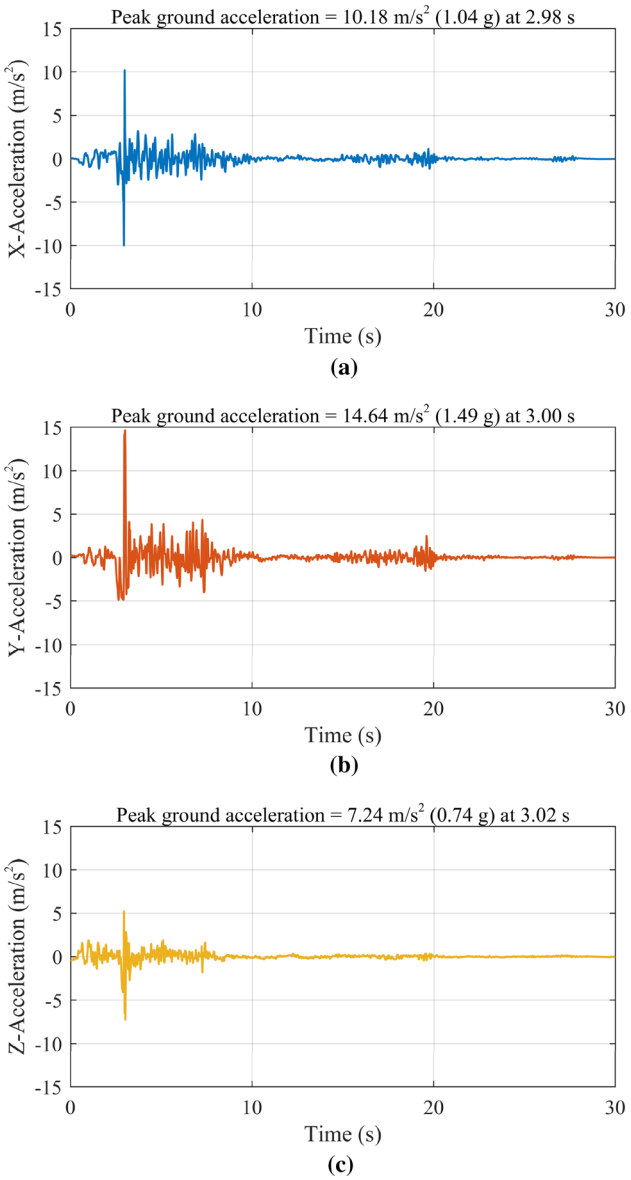

Fig. 5 Accelerogram of seismic signals of the Cape Mendocino earthquake (M_w 7.01, recorded by the Cape Mendocino station) in the: **a** east–west direction, **b** north–south direction and **c** vertical direction

and the gravitational acceleration is 9.8 m/s^2. It is assumed that the slope is subject to the seismic loads of the Cape Mendocino earthquake (the moment magnitude M_w is 7.01), in which there were total 1500 signals recorded by the Cape Mendocino station at a 0.02 s interval (Giardini et al. 2013; Ancheta et al. 2013). The total duration of seismic loading is 29.98 s. Figure 5 gives the accelerograms of seismic accelerations along the three directions. The seismic duration is discretized into a series of time-steps with an interval of 0.02 s, i.e. there are in total 1500 time-steps considered in the following analysis.

3.2 Modelling in BLKLAB

According to the geometrical information of the slope excavation in Fig. 4, the computational domain in BLKLAB is set as 30 m × 30 m × 30 m, as shown in Fig. 6a. According to Table 1, there are in total 28 joint planes generated in the model as shown in Fig. 6a. Due to the infinite extension of joints, the whole computational domain is cut into 384 convex element blocks and each element block forms a complex block, i.e. there are 384 complex blocks in the rock mass (Fig. 6b). Excavation surfaces are treated as special planes in BLKLAB, which are used to cut the original element blocks to regenerate new element blocks after the slope excavation, as shown in Fig. 7a. There are 536 element blocks in total forming 279 complex blocks in the system (Fig. 7b).

3.3 Analysis Results

3.3.1 Removability Analysis

The improved stereo-analytical method is employed to identify geometrically removable blocks around the excavation surfaces. 19 removable blocks are recognized as shown in Fig. 8, among which there are 5 tetrahedral blocks, 6 pentahedral blocks and 8 hexahedral blocks. 13 convex blocks and 6 concave blocks are identified in the blocky rock mass system. The blocks' volumes are given in Table 2, where six blocks are smaller than 1 m^3, five blocks range from 1 to 10 m^3, and eight blocks range from 10 to 100 m^3. Table 2 also gives the potential sliding modes in the form of single-plane and double-plane sliding, where the numbers in the last two columns represent the joint set IDs related to Table 1. For example, block 21 is formed by joints generated by joint sets 1, 2, 3 and 4, and potentially suffers single-plane sliding along joint set 1, 2, 3 or 4 and double-plane sliding controlled by joint pair (1,2), (1,3), (2,4) or (3,4). The following seismic stability analysis is limited to the removable blocks listed in Table 2.

3.3.2 Stability Analysis Under Seismic Loads

If only the block gravity is considered in the stability analysis, all the 19 removable blocks are mechanically stable. Among the removable blocks, 5 blocks (as listed in Table 3) are stable due to frictional resistance and would be unstable if the friction were zero. Table 3 gives the minimum safety factor and the corresponding sliding mode of each block. The other 14 blocks (listed in Table 2 but not in Table 3) are inherently stable under gravity even assuming that all the joints had zero friction.

When the seismic loads are incorporated, the blocks listed in Table 3 are seismically unstable while the other 14 blocks (listed in Table 2 but not in Table 3) are seismically stable.

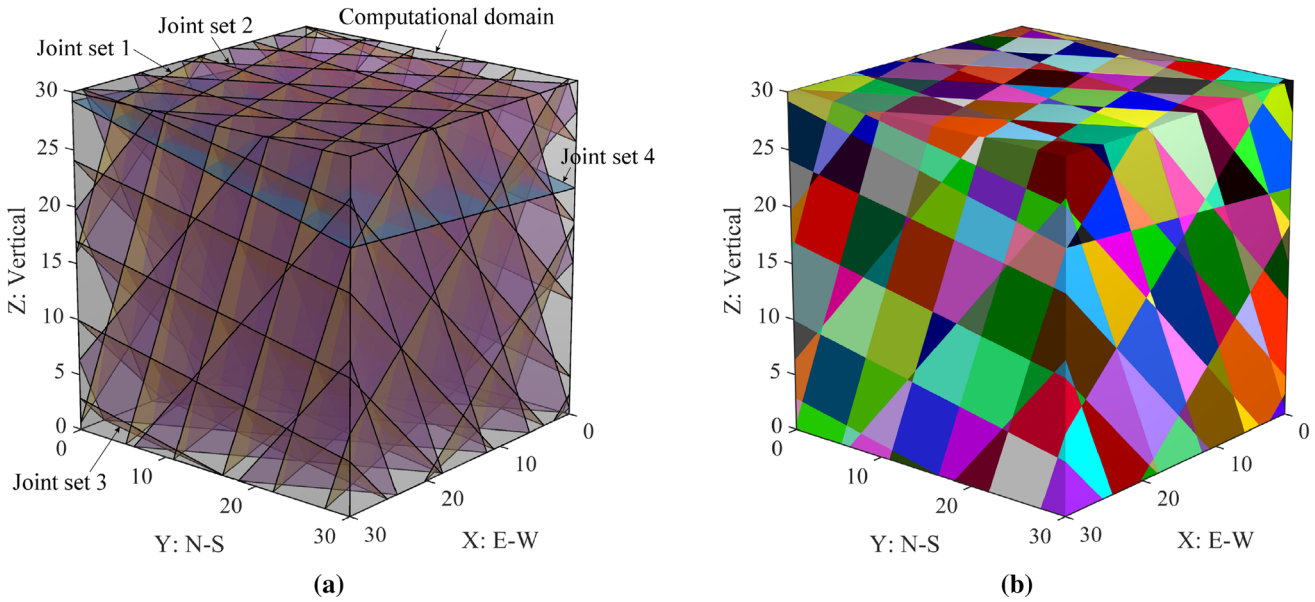

Fig. 6 3D visualization of the blocky rock mass (unit: m): **a** the computational domain and joint sets; **b** the original rock mass before excavation (384 complex blocks)

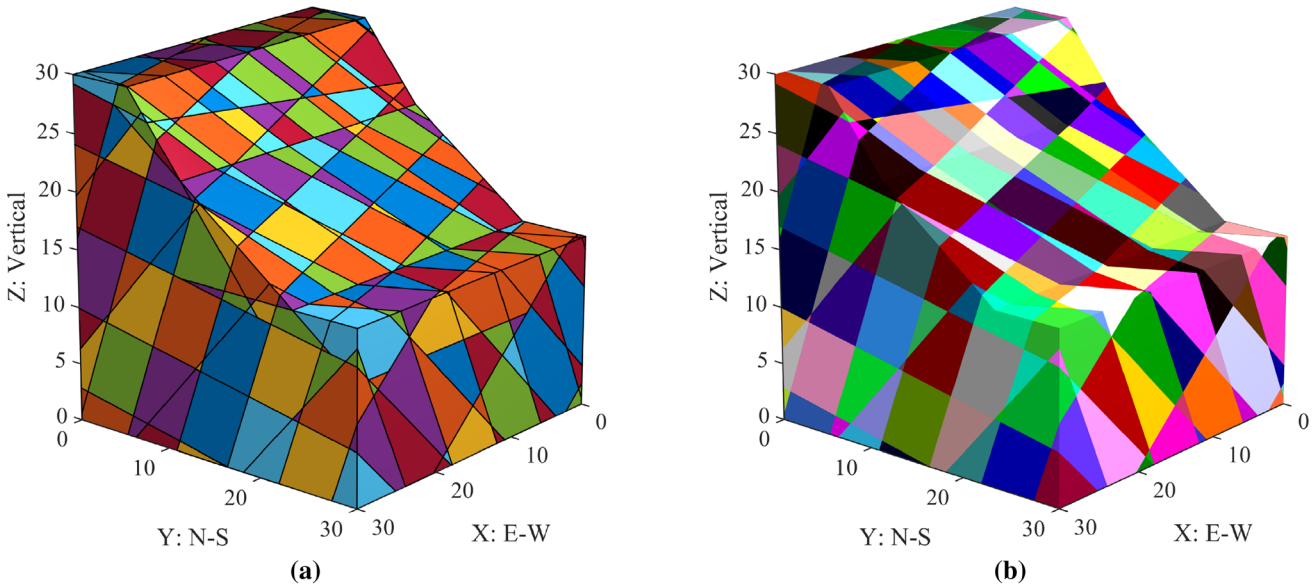

Fig. 7 Visualization of the blocky rock mass after excavation (unit: m): **a** 536 element blocks; **b** 279 complex blocks after regeneration

The seismically unstable blocks are visualized in detail in Fig. 9. Among the seismically unstable blocks, block 89 is the largest in volume. Therefore, it is selected as an example to demonstrate the seismic analysis results. The safety factor of block 89 at each time step can be calculated according to the formulae in Sect. 2.4.2. Figure 10 illustrates the temporal variation of the safety factor of block 89 during the earthquake, where the maximum and minimum safety factors are 3133 at 2.62 s and 0.10 at 2.96 s, respectively. In the time-sequential safety factors, the median value is 1.24, equal to the minimum safety factor in the static analysis. The number of time-steps when the safety factor exceeds 2.5

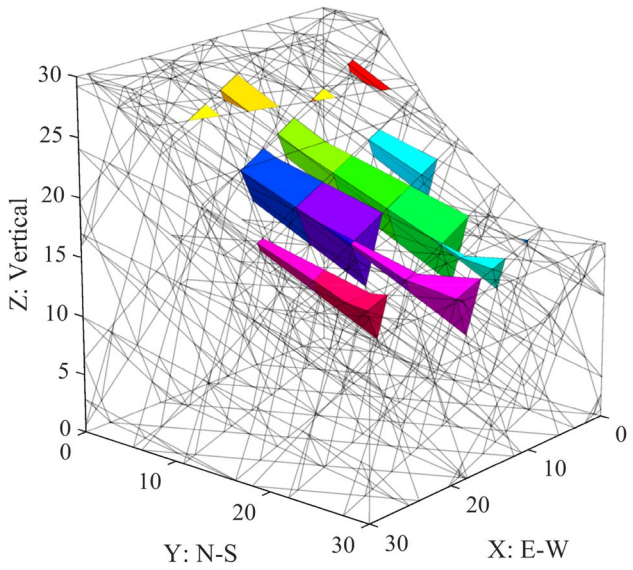

Fig. 8 Removable blocks on the slope excavation surfaces (unit: m)

(about 2 times of 1.24) is 68, i.e. 4.5% of all the time-steps. To clearly show the distribution characteristics of the safety factor, Fig. 11 plots the histogram of the safety factors less than 2.5, where the interval of [1.2, 1.3] has the maximum frequency number of 501. Moreover, the minimum safety factor 1.24 in the static analysis is just located in this interval. Same with the fluctuation of the seismic signals, the safety factor fluctuates more significantly in the early phase of the earthquake than in the later phase. In addition, the safety factor mainly fluctuates around 1.24. The safety factor remains larger than 1 (red dashed line in Fig. 10) after 19.92 s and finally reaches near 1.24. The inset shows an enlarged view of the safety factors between 0 and 4, in which the safety factor fluctuation around 1.24 can be seen clearly. During the earthquake, the seismic loads alter the block stability but do not change the median of the varying safety factor, which is determined by the minimum safety factor in static analysis. This conclusion is also supported by the histograms of safety factor for the other four seismically unstable blocks as shown in Fig. S1 in Online Resource 1 as well as Table 3.

During the earthquake, block 89 may undergo single-plane sliding, double-plane sliding and inherently stable, which are examined in Fig. 12. Herein, the term 'inherently stable' represents that the block is stable under the acting force at a given time step even if there is no restriction by joints. In this case, the safety factor is infinite and not included in Fig. 10. In Fig. 12, the red markers represent unstable cases while the black ones represent stable cases. The mode of double-plane sliding along joint sets 2 and 4 is indicated by a smaller circular marker while the double-plane sliding along joint sets 3 and 4 is by a larger circular marker. The number of time-steps corresponding to different sliding modes is counted in Table 4.

Table 2 Geometrical information of removable blocks around the slope surfaces

Block ID	Volume (m^3)	Number of surfaces	Concavity	Kinematics	
				Single-plane sliding	Double-plane sliding
21	1.3874	5	Convex	1, 2, 3, 4	(1, 2) (1, 3) (2, 4) (3, 4)
75	0.0040	4	Convex	1, 3, 4	(1, 3) (1, 4) (3, 4)
89	7.0242	5	Convex	1, 2, 3, 4	(1, 2) (1, 3) (2, 4) (3, 4)
105	0.2664	5	Convex	1, 2, 3, 4	(1, 2) (1, 3) (2, 4) (3, 4)
138	0.4680	4	Convex	1, 2, 4	(1, 2) (1, 4) (2, 4)
320	32.9903	6	Concave	1, 2, 3	(1, 2) (1, 3)
321	54.9502	5	Convex	1, 2, 3	(1, 2) (1, 3)
322	85.7111	6	Convex	1, 2	(1, 2)
325	0.0088	4	Convex	1, 2, 3	(1, 2) (1, 3) (2, 3)
326	6.1662	6	Concave	1, 2, 3	(1, 2) (1, 3)
331	23.6417	5	Convex	1, 2, 3	(1, 2) (1, 3)
343	0.0167	4	Convex	1, 2, 3	(1, 2) (1, 3) (2, 3)
360	66.1526	6	Concave	1, 2, 3	(1, 2) (1, 3)
362	0.2253	4	Convex	1, 2, 3	(1, 2) (1, 3) (2, 3)
368	99.1481	6	Convex	1, 2	(1, 2)
370	4.2937	6	Concave	1, 2, 3	(1, 2) (1, 3)
371	37.4186	6	Concave	1, 2, 3	(1, 2) (1, 3)
377	7.6465	5	Convex	1, 2, 3	(1, 2) (1, 3)
383	24.0377	6	Concave	1, 2, 3	(1, 2) (1, 3)

Note: the numbers in the last two columns related to kinematics modes indicate the relevant joint set IDs

Table 3 Static and seismic analysis results

Block ID	Volume (m^3)	Results without seismic loads (i.e. only gravity is considered)		Results with seismic loads	
		Sliding plane (s)	Minimum Safety factor	Instability probability (%)	Probabilistic instability volume (m^3)
21	1.3874	4	1.24	11.13	15.44×10^{-2}
75	0.0040	(3, 4)	1.59	5.20	0.021×10^{-2}
89	7.0242	4	1.24	11.13	78.18×10^{-2}
105	0.2664	4	1.24	11.13	2.97×10^{-2}
138	0.4680	4	1.24	12.13	5.68×10^{-2}
Blocky rock mass system	9.1500	–	–	11.18	102.28×10^{-2}

Note: the numbers in the column of sliding plane(s) indicate the relevant joint set IDs

In addition to the stability status, the seismic loads also alter the kinematic modes of the rock block during an earthquake.

Among all the 1500 time-steps, the safety factor of block 89 is less than 1 at 167 time-steps, while it is stable at the other instances. The instability probability of block 89 can thus be derived as $167/1500\times100\%=11.13\%$. According to Eq. (22), the probabilistic instability volume of block 89 is calculated as $7.0242\times11.13\%=0.7818$ m^3. Similarly, the evaluation parameters of blocks 21, 75, 105 and 138 are calculated and listed in Table 3. The statistics of the kinematics and safety factor during the earthquake for these four blocks are given in Table S1 (Online Resource 1). The total volume of seismically unstable blocks is 9.1500 m^3 and the probabilistic instability volume of the blocky rock mass system is 1.0228 m^3 according to Eq. (23). Based on Eq. (24), the instability probability of this blocky rock mass system is derived as $1.0228/9.1500\times100\%=11.18\%$.

3.3.3 Influences of the Earthquake Parameters on Slope Stability Under Seismic Loads

We investigate the influences of earthquakes parameters (moment magnitude M_w and epicentral distance R_{epi}) on the stability of the blocky rock mass system as shown in Fig. 7. Sufficient quantity of acceleration sequences of earthquakes is crucial for the analysis here. Usually, an earthquake is recorded by several stations and the acceleration signals captured by different stations are different. Thus, we select a series of seismic signals of different earthquakes recorded by different seismic stations. The data herein are from the Pacific Earthquake Engineering Research Center (PEER) ground motion database (Yenier et al. 2010; Giardini et al. 2013; Ancheta et al. 2013), among which 19 earthquakes with at least 23 recorded sequences and 11 seismic stations with at least 7 earthquakes recorded are selected in this paper. The total number of acceleration sequences is 1098, i.e. 19 earthquakes have 1015 sequences by different stations and 11 stations have 83 sequences of different earthquakes. The information of earthquakes and stations is given in Online Resource 2. The interval of time-sequential accelerations, which is determined by the sampling frequency of the station, varies at different stations. To unify the input earthquake signals, all the accelerations are resampled at an interval of 0.02 s using an open-source code OpenSeismoMatlab (Papazafeiropoulos and Plevris 2018). In addition, the signals are transformed into the standard x, y and z directions according to Eq. (3). The moment magnitudes M_w of the selected earthquakes ranges from 4.53 to 7.62 and the epicentral distance R_{epi} ranges from 2.47 to 557.63 km (Tables S2 and S3 in Online Resource 1) as shown in Fig. 13. In general, a stronger earthquake has a higher chance to be recorded by a seismic station located far from the epicenter.

3.3.3.1 Influences of Earthquake Magnitude M_w

The probabilistic instability volume V^u and instability probability P^u of the blocky rock mass under different earthquakes are shown in Fig. 14. For the Big Bear-02 earthquake (M_w 4.53), the probabilistic instability volume is 0, indicating that there is no seismically unstable block on the slope. Thus, Eq. (24) cannot be used to calculate the instability probability of the rock system. In this case, the instability probability is denoted as 0 as shown in Fig. 14b. The maximum V^u and P^u both occur during the Imperial Valley-06 earthquake with values of 2.039 m^3 and 22.29%, respectively. Generally, the two parameters vary more significantly with the earthquake magnitude and are likely to have larger values under stronger earthquakes; thus, a larger earthquake has the potential to

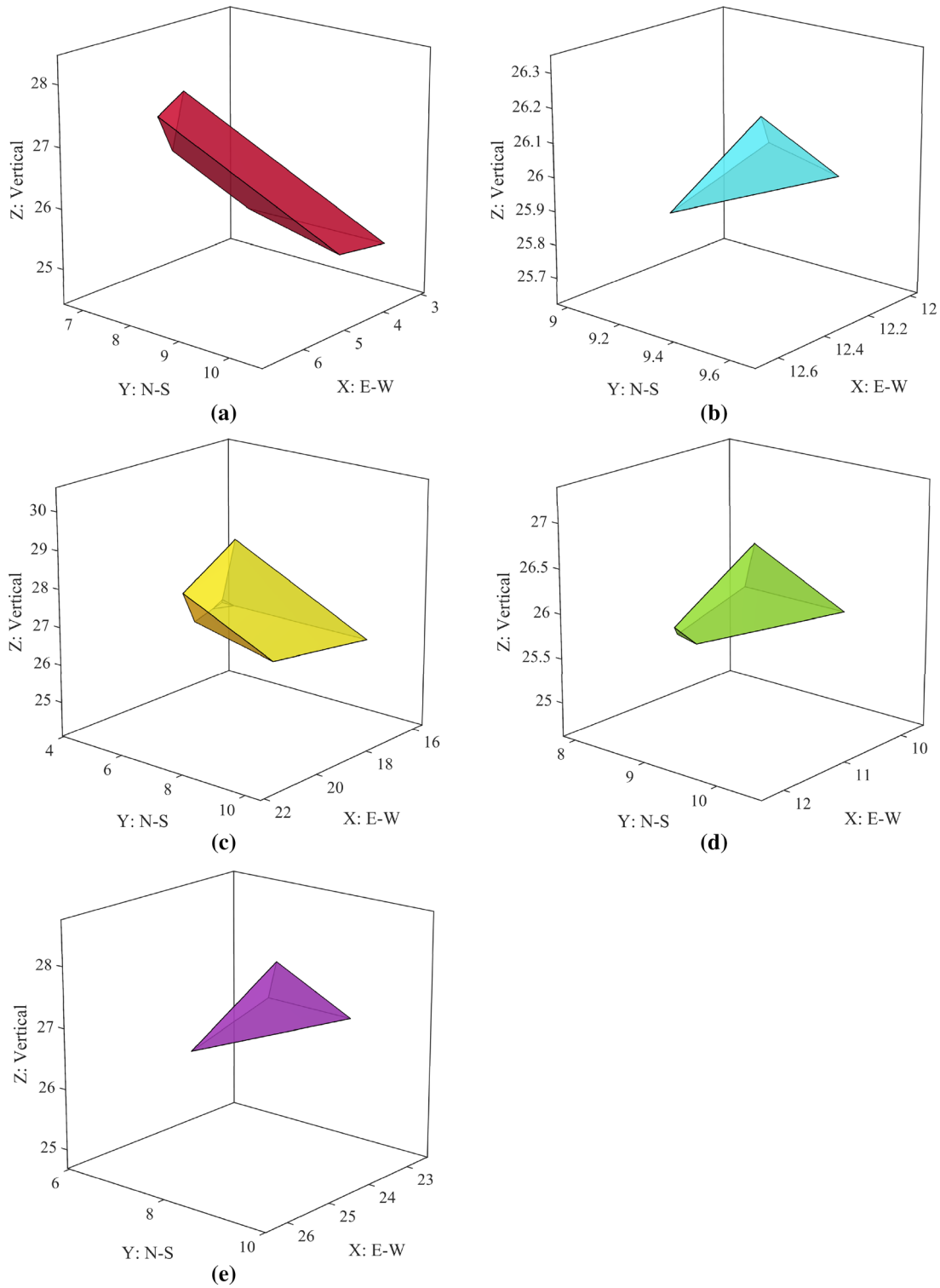

Fig. 9 Detailed visualization of seismically unstable blocks in the blocky rock mass system (Unit: m): **a** block 21; **b** block 75; **c** block 89; **d** block 105; **e** block 138

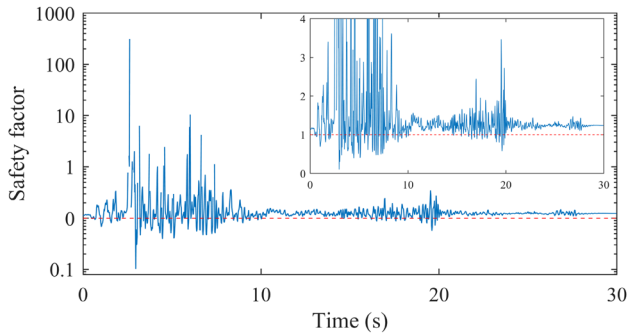

Fig. 10 Variation of safety factor of block 89 during the earthquake

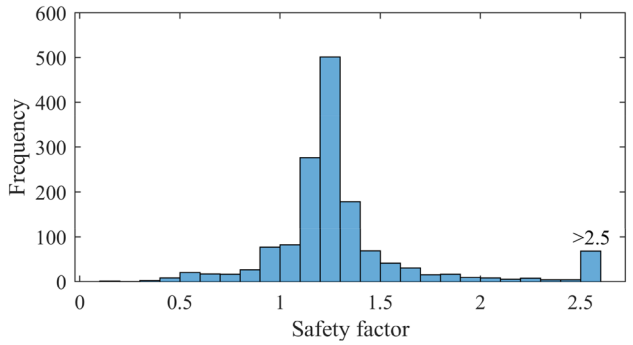

Fig. 11 Histogram of time-sequential safety factor of block 89 during the earthquake

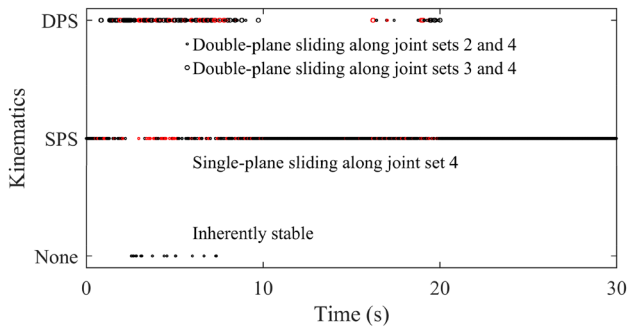

Fig. 12 Kinematics of block 89 during the earthquake (red markers represent unstable cases while black markers represent stable cases; DPS and SPS indicate the double-plane sliding and single-plane sliding modes, respectively)

induce a higher instability probability and more hazardous rock mass failure. Interestingly, as shown in Fig. 14, the values of the two parameters towards the upper end seem to be bounded by a linear trend. Of course, the data are highly scattered, but such an estimated upper boundary for the evaluation parameters may still be very useful for designing support systems against possible earthquake scenarios in rock engineering.

Table 4 Quantity statistics of time-steps in different kinematics

Sliding plane(s)	Total	Unstable	Stable
(2,4)	124	16	108
(3,4)	141	38	103
4	1215	113	1102
None	20	–	–

Note: 'None' represent the block is inherently stable under the acting force at this time step

3.3.3.2 Influences of Epicentral Distance R_{epi}

The energy of seismic waves radiated from the earthquake fault decays as they propagate in the crust due to various attenuation mechanisms such as geometrical spreading, elastic scattering and anelastic dissipations (Stein and Wysession 2003). Thus, it is essential to investigate the influences of the epicentral distance R_{epi} on the slope stability under seismic loads. Figure 15 shows the variations of V^{μ} and P^{μ} as a function of R_{epi}. It is clear that larger V^{μ} and P^{μ} occur in regions closer to the epicenter, especially if R_{epi} less than ~ 50 km. Only strong earthquakes (e.g. Chi-Chi with M_w 7.62, Kocaeli with M_w 7.51, Landers with M_w 7.28 and Loma Prieta with M_w 6.93) cause higher instability probability and more hazardous failure in regions beyond ~ 50 km from the epicenter. The two parameters both decrease with R_{epi}. Despite of the strong fluctuation of data points, one may still observe a general power law decay trend of V^{μ} and P^{μ} as a function of R_{epi} (see the insets of Fig. 15). In addition, the values of the two parameters towards the upper and lower ends seem to be bounded by two lines on the log–log plot as shown in the insets of Fig. 15. Compared with Fig. 14, it seems that the distance has an even more significant impact on the slope stability under seismic loads than the earthquake magnitude. The decay of instability probability to R_{epi} is compatible with the often observed decay of aftershock density with the epicentral distance (Felzer and Brodsky 2006).

3.3.4 Influences of the Local Site Effect on Slope Stability Under Seismic Loads

Another important factor that needs to be examined is the local site effect, which has been reported to have strong controls on the ground motion (Civelekler et al. 2021; Holt et al. 2019). Thus, the recorded seismic signals are, to some extent, dependent on the geological and geotechnical conditions of the site where the seismic stations are located

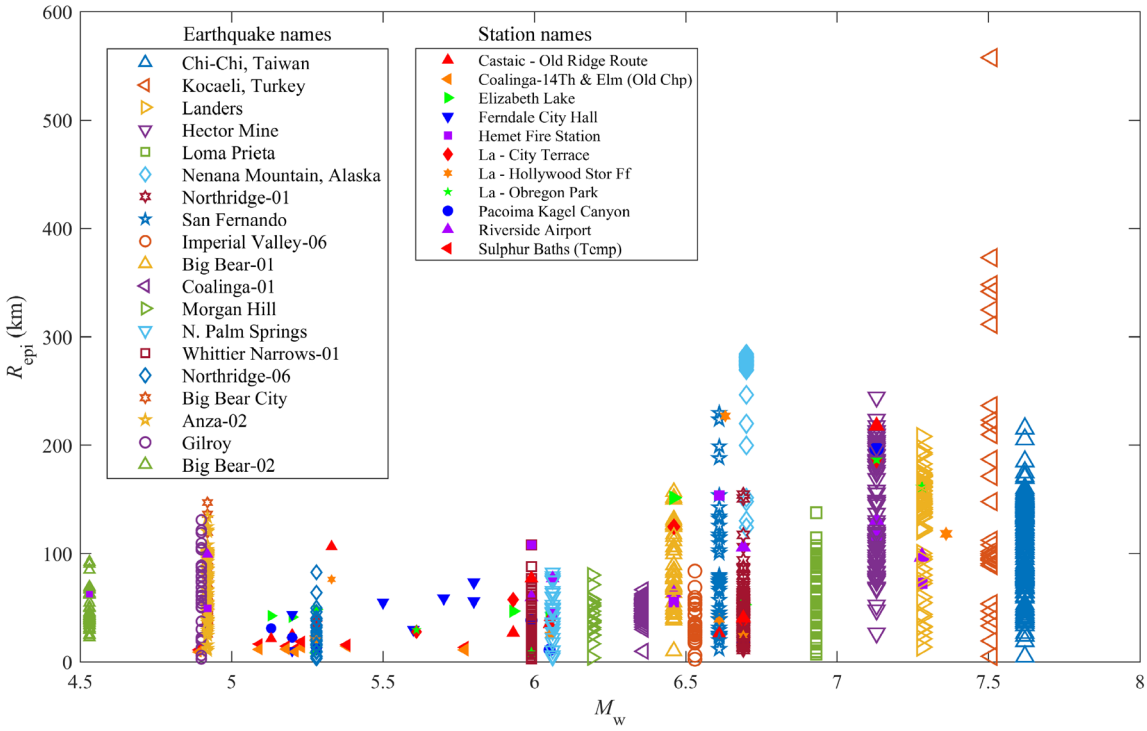

Fig. 13 Magnitude M_w and epicentral distance R_{epi} of the selected earthquakes. The empty markers indicate the sequences of some earthquakes by different stations and the filled ones represent sequences of different earthquakes recorded by the same station

(Zafarani et al. 2020). Taking Loma Prieta earthquake with M_w 6.93 as an example (Fig. 16), there are two seismic stations located 96.34 and 96.52 km away from the epicenter while the instability probability parameters are 1.01% and 19.63%, highlighted by the dark empty marker and the red filled marker in Fig. 16, respectively. For a wider range of 95–100 km away from the epicenter, the instability probability varies from 0.82 to 19.63%. On the other hand, Fig. 17a shows the instability probability of the rock system as a function of the earthquake magnitude, where the P^u values are quite different in different earthquakes even though they are recorded by the same seismic station. For every station in Fig. 17b, P^u varies with earthquakes of different distances from the station. In general, the trends in Fig. 17 are consistent with those observed in Figs. 14b and 15b.

4 Discussion and Concluding Remarks

This paper proposed a generalized block theory by combining the pseudo-static method and the traditional block theory to evaluate the seismic stability of rock blocks and blocky rock mass systems, taking the advantages of both methods. The proposed method used the safety factor to identify the stable status of rock blocks over time and calculate the instability probability to evaluate the stability of blocky rock masses under seismic loads, which is computationally efficient compared to many other methods (e.g. finite element method or discrete element method). The treatment of seismic loads herein is still in the context of pseudo-static method and thus our GBT method gives an approximation to the transient process within each time step. Following the basic assumptions of the original block theory, the GBT focuses on rigid blocks of three kinematic modes, i.e. free translation, single-plane sliding and double-plane sliding. As a result, the GBT does not consider the deformation and breakage of rock blocks which may occur during actual dynamic progresses. The Newmark method (Jibson 2011; Fu et al. 2019), discrete element method using deformable blocks (Cundall 1988; Gischig et al. 2016) or other more sophisticated analysis approaches may be needed if more detailed dynamic response of rock blocks during earthquakes are to be considered (Zhang 2018).

Our paper proposed two evaluation parameters to quantify the instability status and the hazardousness of blocky rock masses under earthquakes: instability probability and probabilistic instability volume. It is found that the proposed parameters generally have a positive relationship with the earthquake magnitude and an inverse power law relationship with the epicentral distance. The proposed stability

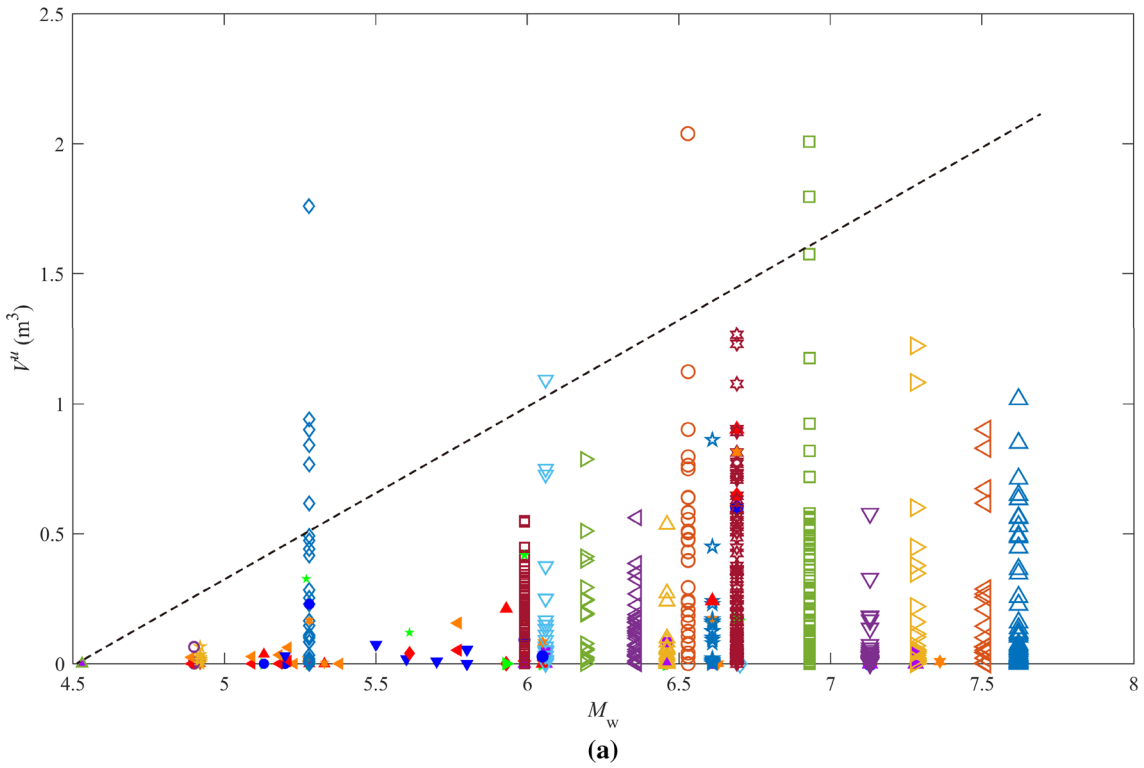

(a)

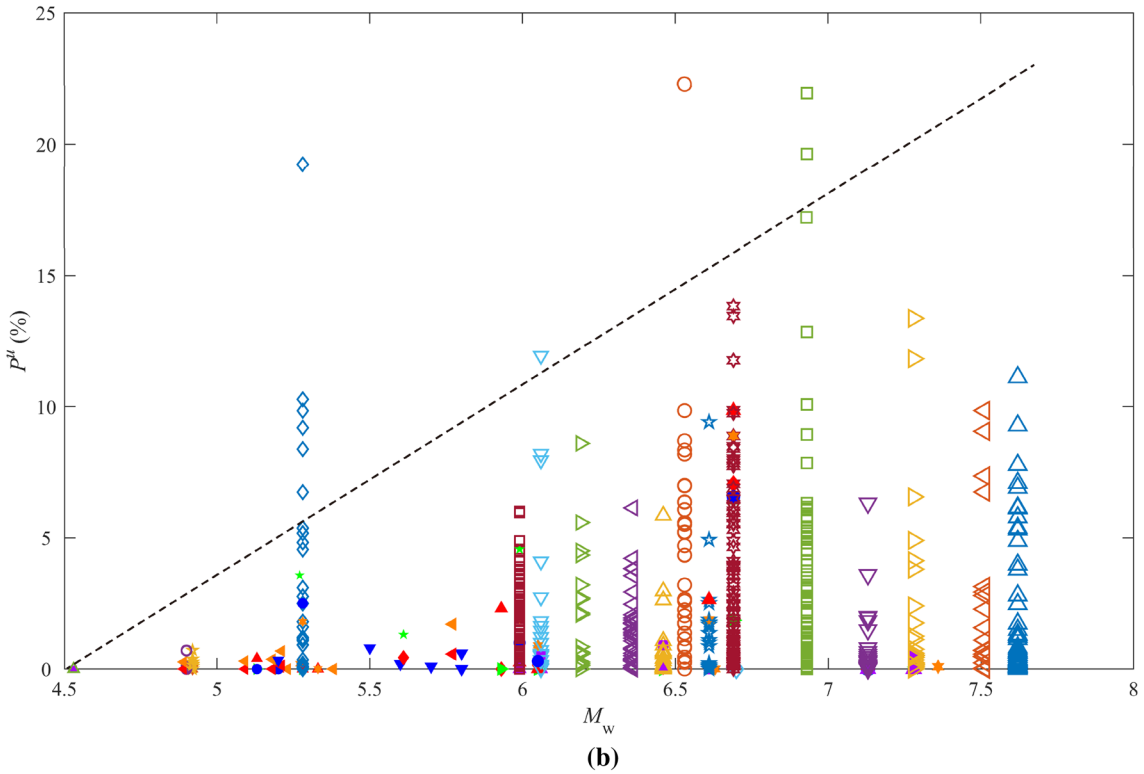

(b)

Fig. 14 **a** Probabilistic instability volume and **b** instability probability of the blocky rock mass system subject to earthquakes with different magnitudes. Refer to Fig. 13 for the legend

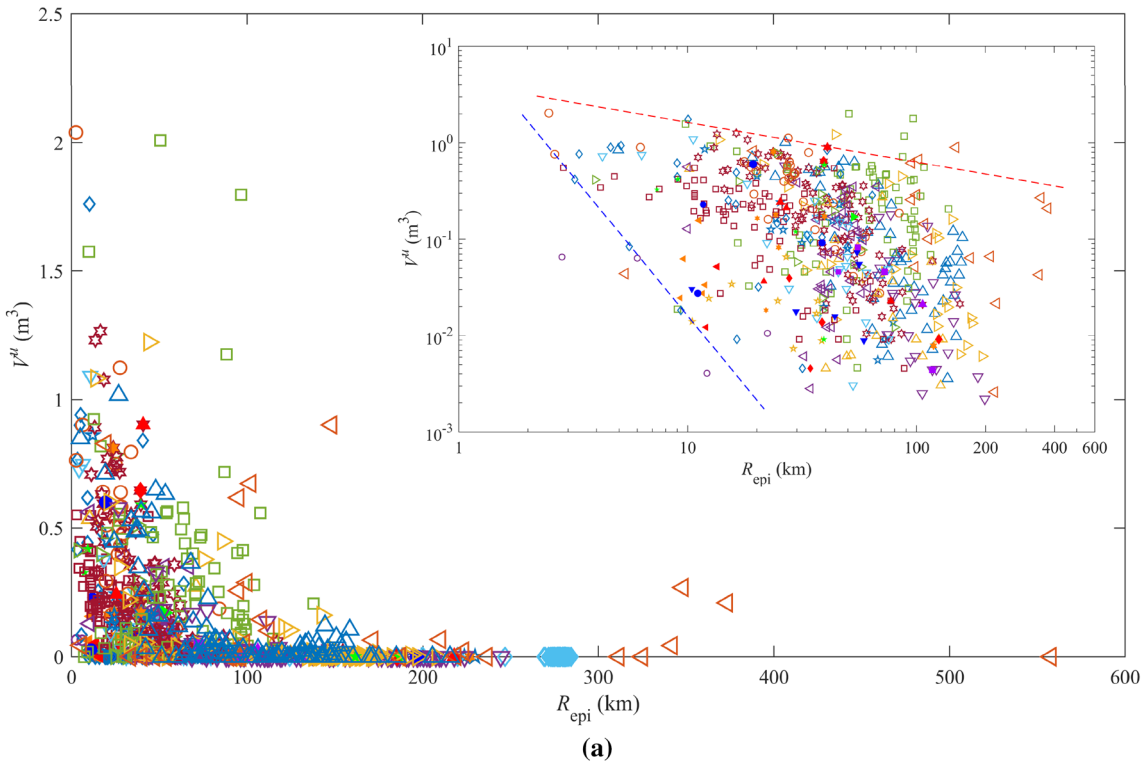

Fig. 15 **a** Probabilistic instability volume and **b** instability probability of the blocky rock mass system as a function of the epicentral distance. Refer to Fig. 13 for the legend

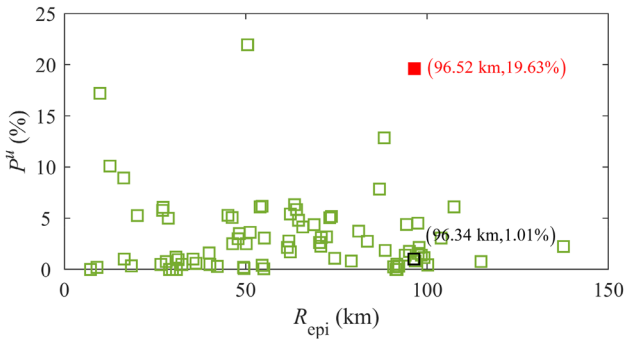

Fig. 16 P^u as a function of R_{epi} for the Loma Prieta earthquake with $M_w = 6.93$

parameters are intuitional and simple for practitioners to understand and use in rock engineering. Once the parameters of a blocky rock mass are evaluated with the GBT, we could determine the relationship between the evaluation parameters and the earthquake parameters (e.g. earthquake magnitude and epicentral distance), which will help predict the instability probability and hazardousness of the blocky rock mass as well as design the support systems.

To sum up, our proposed method consists of three primary procedures: (1) generating a geometrical model of the blocky rock mass system, (2) analyzing the geometrical removability and identifying the geometrically probable sliding modes of rock blocks with the improved stereo-analytical method, (3) determining the evaluation parameters for seismic stability of removable blocks and the blocky rock mass system. In the stability analysis, the basic safety factors for three kinematic modes were derived considering time-varying seismic loads, which determines the stability of a rock block over time. Two new parameters, i.e. instability probability P^u and probabilistic instability volume V^u, were proposed to evaluate the seismic stability of rock blocks. The instability probability P^u was defined as the ratio of the time for a block becoming unstable to the total seismic loading time, and the probabilistic instability volume V^u was the product of instability probability and block volume. A rock block was defined as a seismically unstable block if its instability probability is larger than 0. As for a blocky rock mass system, its probabilistic instability volume is the sum of V^u of all seismically unstable blocks and the instability probability is the ratio of its probabilistic instability volume and total volume of seismically unstable blocks. These parameters can reflect the instability probability and hazardousness of blocky rock mass systems under earthquake activities. The proposed methodology has been implemented in our in-house BLKLAB platform and used to investigate the seismic stability of a generic slope excavation under different earthquakes. The simulation results showed that the earthquake loads may both alter the stability status and kinematic modes of rock blocks. As for the blocky rock mass system, a stronger earthquake produces a higher instability probability and a larger probabilistic instability volume. In addition, the two evaluation parameters both decay with the epicentral distance, in general following an inverse power law trend. It is found that the local site effect also strongly affects the slope stability under seismic loads.

Appendix A: Comparative Analysis of BLKLAB and 3DEC

Initial Stability Status Subject to Gravity

For the comparison purpose, we build a model in 3DEC using exactly the same configuration as that in BLKLAB (as described in Sect. 3.1). Since the GBT follows the rigid block assumption of the traditional block theory (Goodman and Shi 1985), the 3DEC model also assumes blocks are rigid. The model in 3DEC utilizes the Coulomb slip model to simulate joints, of which the parameters are listed in Table 1. In addition, the cohesion of joints is set as 0, and the normal and shear stiffnesses have an equal value of 10 GPa/m. The 3DEC model uses roller boundary conditions on the side and bottom boundaries while the upper boundary is a free surface. The geometrical model and the initial displacement field after geo-stress initialization in 3DEC are shown in Fig. 18a and b, respectively. The maximum magnitude of the block displacement is about 8.03×10^{-4} m. In 3DEC, we could also calculate the safety factor of joints in a rigid blocky rock mass system based on the strength reduction method, which gives the minimum safety factor of the system (3DEC Manual 2019). It should be noted that the safety factor calculation should be executed after the geo-stress initialization. The initial safety factor of the 3DEC model is 1.0, i.e. the slope is initially stable, which is smaller than the safety factor (1.24 or 1.59 as shown in Table 3) obtained by BLKLAB. The difference between the two software platforms is attributed to the different calculation algorithms. The GBT in BLKLAB only solves the safety factor of removable blocks and ignores other blocks that may be secondary unstable blocks (Noroozi et al. 2012; Fu and Ma 2014). As a contrary, 3DEC loop all the blocks to fetch a minimum safety factor of the rock system.

Time-Sequential Safety Factors of the Rock System Under Seismic Loads

Within the scope of pseudo-static method (Zhang 2018), the time-sequential safety factor of the rock system under

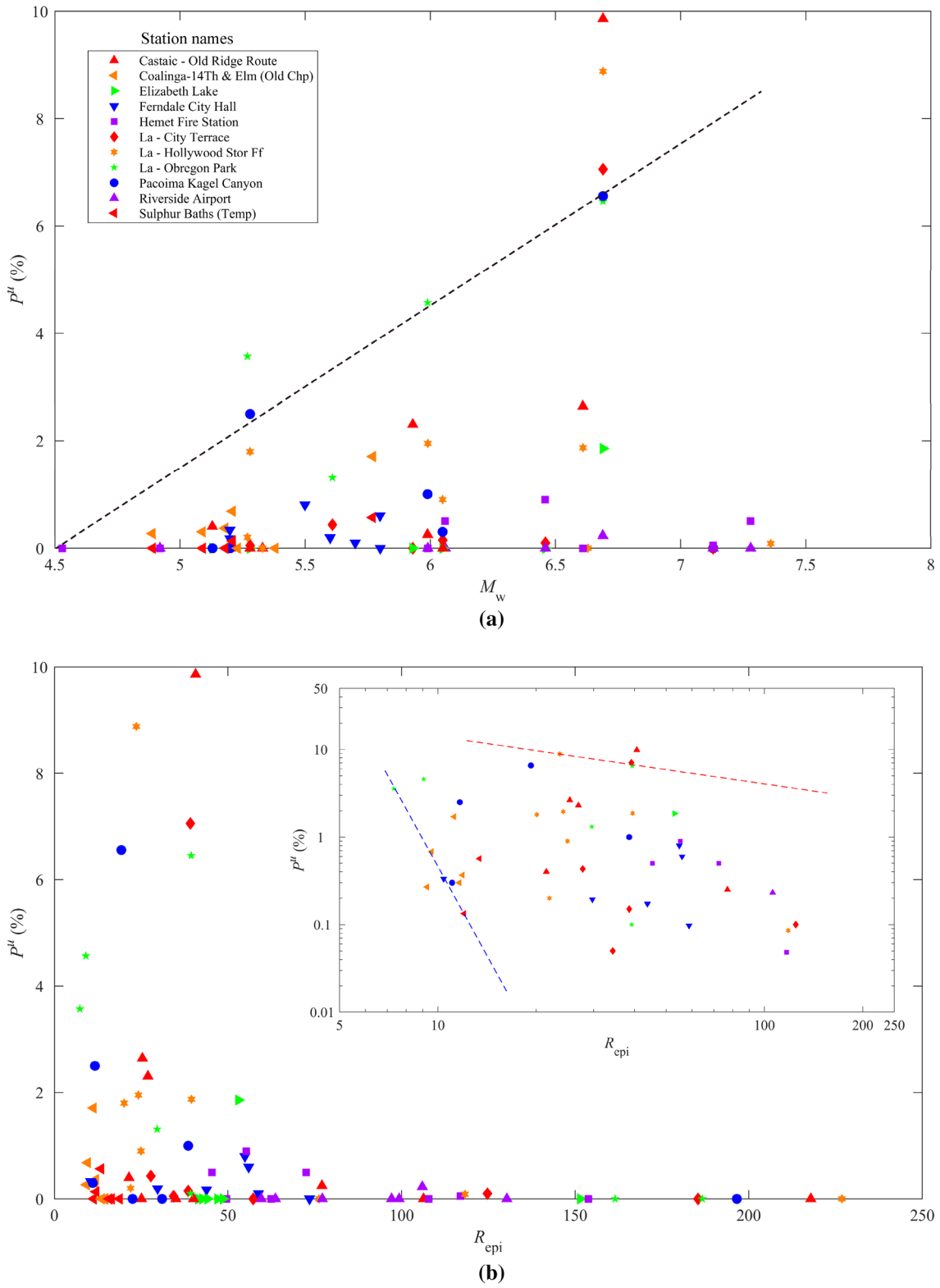

Fig. 17 Instability probability of the blocky rock mass system as a function of **a** the earthquake magnitude and **b** the epicentral distance for different earthquake acceleration sequences recorded by the same seismic station

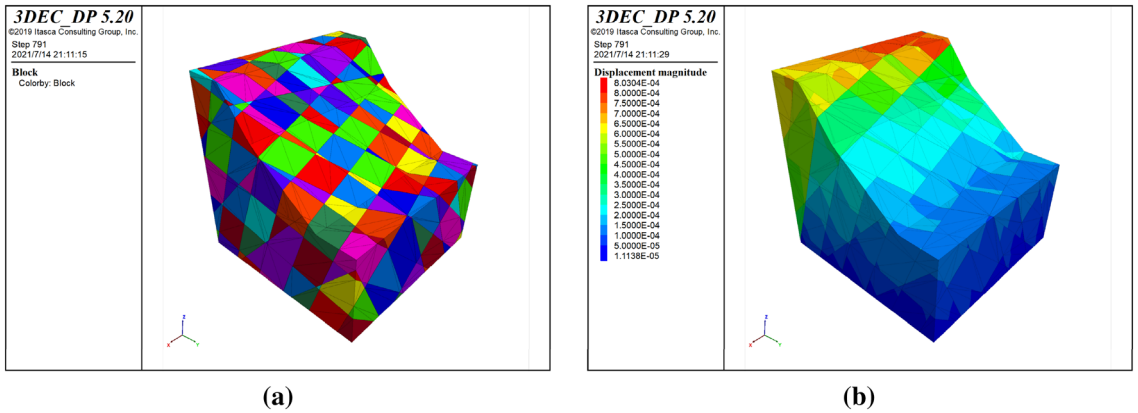

Fig. 18 The 3DEC model of a blocky rock slope: **a** the geometrical model; **b** the initial displacement field after geo-stress initialization

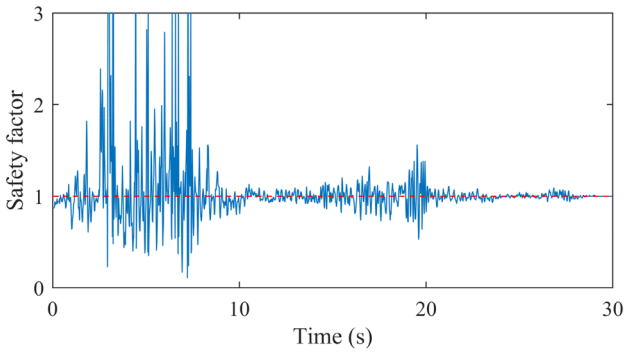

Fig. 19 Time-sequential safety factors of the rock slope system calculated by the 3DEC

Table 5 Earthquakes information

Earthquake name	Years	M_w	Station name	Original interval (s)
Drama, Greece	1985	5.20	Drama (Bsmt)	0.0024
Santa Barbara	1978	5.92	Santa Barbara Courthouse	0.01
N. Palm Springs	1986	6.06	Hurkey Creek Park	0.005
Parkfield	1966	6.19	Cholame-Shandon Array #12	0.01
Imperial Valley	1979	6.53	El Centro Array #8	0.005
San Fernando	1971	6.61	Castaic-Old Ridge Route	0.01
Spitak, Armenia	1988	6.77	Gukasian	0.01
Kobe, Japan	1995	6.90	Takarazuka	0.01
Loma Prieta	1989	6.93	Gilroy Array #3	0.005
Cape Mendocino	1992	7.01	Cape Mendocino	0.02
Kocaeli, Turkey	1999	7.51	Yarimca	0.005

seismic loads in 3DEC is also calculated by altering the resultant force $\mathbf{F}^{a,t}$ derived in Eq. (4). The sequential safety factor of the rock system subject to the Cape Mendocino earthquake (M_w 7.01 as shown in Fig. 5; Giardini et al. 2013) is illustrated in Fig. 19. The minimum safety factor during the earthquake is 0.11 at 7.22 s, which is close to the one given by BLKLAB, i.e. 0.1 at 2.62 s. This consistency indicates that the removable blocks resolved by GBT are indeed the controlling parts of the slope under seismic loads. Similar to the GBT results shown in Figs. 5 and 10, the safety factor derived by 3DEC fluctuates more significantly in the early phase of the earthquake than in the later phase. Among all the 1500 time-steps, there are 717 time-steps with the safety factor less than unity. According to Eq. (21), the instability probability of the rock system in 3DEC model is calculated as 717/1500 = 47.89%, which is larger than the result given by BLKLAB, i.e. 11.18%. The smaller safety factor and higher instability probability in 3DEC imply that the discrete element method gives a more conservative evaluation for the rock system under seismic loads than the GBT. However, the GBT is capable of determining the exact location of unfavorable blocks during the earthquake and their kinematic modes. In addition, the GBT has a higher computational efficiency since it does not require any contact detection and interaction calculation.

Relationship Between the Instability Probability and Earthquake Magnitude

We then select 11 earthquakes (Yenier et al. 2010; Giardini et al. 2013; Ancheta et al. 2013) with the moment magnitude ranging from 5.20 to 7.51 as a database to investigate the sensitivity of the GBT and 3DEC results to the earthquake magnitude. We choose the time series of signals recorded by several representative stations for each earthquake as listed in Table 5. All the acceleration signals, resampled to 0.02 s and transformed into the standard directions, are plotted in Fig. 20. The instability

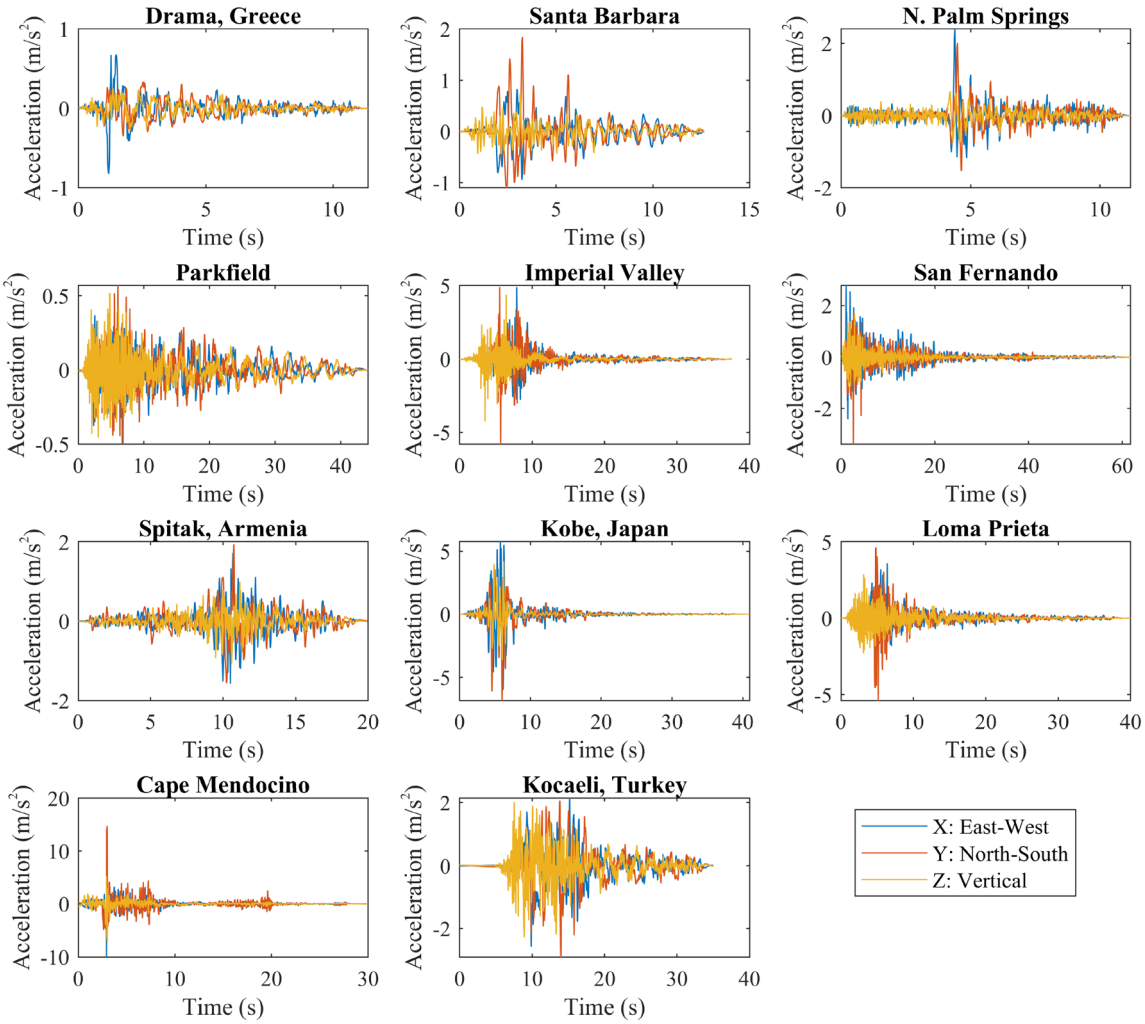

Fig. 20 Ground accelerations monitored during different earthquakes

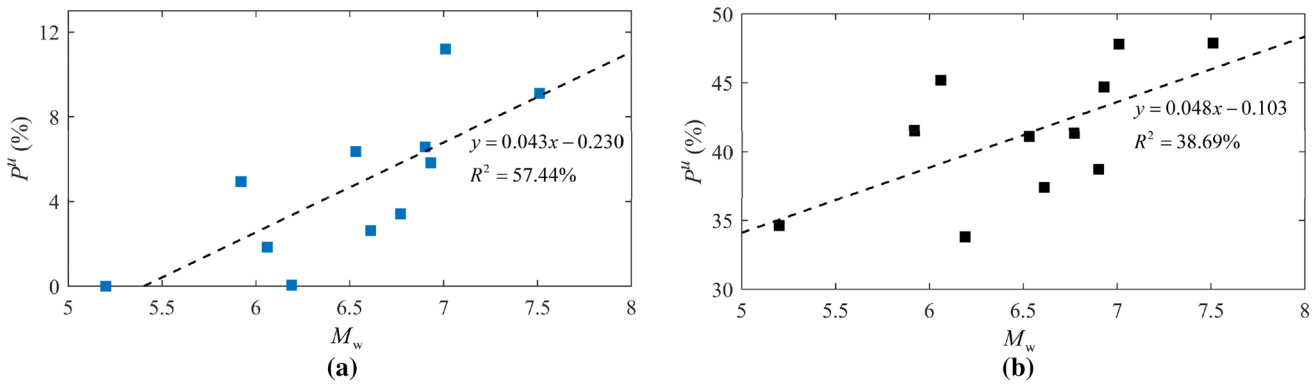

Fig. 21 Instability probability of the blocky rock mass under different earthquakes calculated by **a** the BLKLAB and **b** the 3DEC models

probabilities of the rock system by 3DEC and BLKLAB are shown in Fig. 21a and b, respectively, where they both tend to exhibit a positive linear correlation with the earthquake magnitude. The aforementioned results support the validity and effectiveness of our proposed GBT method for analyzing blocky rock mass stability under seismic loads.

Supplementary Information The online version contains supplementary material available at https://doi.org/10.1007/s00603-021-02628-3.

Acknowledgements The research was supported by the National Natural Science Foundation of China (Grant No. 52008307), the National Natural Science Foundation of China (Grant No. 41961134032) and the Swiss National Science Foundation (Grant No. 189882). The first author would like to acknowledge the funding by the China Postdoctoral Science Foundation (Grant No. 2021T140517). The authors also acknowledge the Pacific Earthquake Engineering Research Center (PEER) for the access to their datasets.

References

3DEC Manual (2019) 3 Dimensional distinct element code manual 5.0. Itasca Consulting Group, Inc, Minneapolis

Ancheta TD, Darragh RB, Stewart JP et al. (2013) PEER report on "PEER NGA-West2 Database". Pacific Earthquake Engineering Research Center, University of California, Berkeley. https://apps.peer.berkeley.edu/publications/peer_reports/reports_2013/webPEER-2013-03-Ancheta.pdf. (**Accessed 12 Jun 2021**)

Bakun-Mazor D, Hatzor YH, Glaser SD (2012) Dynamic sliding of tetrahedral wedge: the role of interface friction. Int J Numer Anal Meth Geomech 36:327–343

Civelekler E, Okur VD, Afacan KB (2021) A study of the local site effects on the ground response for the city of Eskişehir, Turkey. Bull Eng Geol Environ 80:5589–5607

Cundall PA (1988) Formulation of a three-dimensional distinct element model part I. A scheme to detect and represent contacts in a system composed of many polyhedral blocks. Int J Rock Mech Min Sci Geomech Abstr 25(3):107–116

Felzer KR, Brodsky EE (2006) Decay of aftershock density with distance indicates triggering by dynamic stress. Nature 441:735–738

Fu GY, Ma GW (2014) Extended key block analysis for support design of blocky rock mass. Tunn Undergr Space Technol 41:1–13

Fu XD, Sheng Q, Tang H, Chen J, Du YX, Zhang ZP, Mei HR (2019) Seismic stability analysis of a rock block using the block theory and Newmark method. Int J Numer Anal Meth Geomech 43:1392–1409

Ghosh A, Haupt W (1989) Computation of the seismic stability of rock wedges. Rock Mech Rock Eng 22(2):109–125

Giardini D, Woessner J, Danciu L et al (2013) Seismic Hazard Harmonization in Europe (SHARE): online data resource. Eur Facilities Earthquake Hazard Risk. https://doi.org/10.12686/SED-00000001-SHARE (**Accessed 12 Jun 2021**)

Gischig V, Preisig G, Eberhardt E (2016) Numerical investigation of seismically induced rock mass fatigue as a mechanism contributing to the progressive failure of deep-seated landslides. Rock Mech Rock Eng 49:2457–2478

Goodman RE, Shi GH (1985) Block theory and its application to rock engineering. Prentice Hall, New Jersey

Hoek E (1983) Strength of jointed rock masses. Géotechnique 33(3):187–223

Hoek E, Brown ET (1997) Practical estimates of rock mass strength. Int J Rock Mech Rock Min 34(8):1165–1186

Holt J, Edwards B, Poggi V (2019) Scenario-dependent site effects for the determination of unbiased local magnitude. Bull Seismol Soc Am 109(6):2658–2673

Jia C, Li Y, Lian MY, Zhou XY (2017) Jointed surrounding rock mass stability analysis on an underground cavern in a hydropower station based on the extended key block theory. Energies 10(4):563

Jibson RW (2011) Methods for assessing the stability of slopes during earthquakes—a retrospective. Eng Geol 122(1–2):43–50

Kulatilake PHSW, Wang LQ, Tang HM, Liang Y (2011) Evaluation of rock slope stability for Yujian River dam site by kinematic and block theory analyses. Comput Geotech 38(6):846–860

Law HK, Lam IP (2003) Evaluation of seismic performance for tunnel retrofit project. J Geotech Geoenviron Eng 129(7):575–589

Li JY, Xue J, Xiao J, Wang Y (2012) Block theory on the complex combinations of free planes. Comput Geotech 40:127–134

Liu TX, Deng JH, Zheng J, Zheng L, Zhang ZH, Zheng HC (2017) A new semi-deterministic block theory method with digital photogrammetry for stability analysis of a high rock slope in China. Eng Geol 216:76–89

Mousavi SM, Beroza GC (2020) A machine-learning approach for earthquake magnitude estimation. Geophys Res Lett 47(1):e2019GL085976

Newmark NM (1965) Effects of earthquakes on dams and embankments. Géotechnique 15(2):139–160

Noroozi M, Jalali SE, Yarahmadi Bafghi AR (2012) 3D key-group method for slope stability analysis. Int J Numer Anal Meth Geomech 36(16):1780–1792

Papazafeiropoulos G, Plevris V (2018) OpenSeismoMatlab: a new open-source software for strong ground motion data processing. Heliyon 4:e00784

Prasad VVR, Dwivedi RD, Swarup A (2013) Determination of support pressure for tunnels and caverns using block theory. Tunn Undergr Space Technol 37:55–61

Rocscience SWedge (2020) Seismic force in SWedge. Rocscience SWedge Online Help. https://www.rocscience.com/help/swedge/swedge/seismic_force.htm. (**Accessed 12 Jun 2021**)

Rocscience UnWedge (2020) Seismic force in UnWedge. Rocscience UnWedge Online Help. https://www.rocscience.com/help/unwedge/unwedge/seismic_force.htm. (**Accessed 12 Jun 2021**)

Roy R, Ghosh D, Bhattacharya G (2016) Influence of strong motion characteristics on permanent displacement of slopes. Landslides 13(2):279–292

Shi GH (1988) Discontinuous deformation analysis: a new numerical model for the statics and dynamics of block systems. Dissertation, University of California

Stein S, Wysession M (2003) An introduction to seismology, earthquakes, and earth structure. Blackwell Publishing, Hoboken

Terzaghi K, Peck RB, Mesri G (1996) Soil mechanics in engineering practice, 3rd edn. John Wiley & Sons, Hoboken

Tonon F (2020) Simplified consideration for permanent rock dowels in block theory and 2-D limit equilibrium analyses. Rock Mech Rock Eng 53:2001–2006

Wang SF, Zhang ZX, Huang X, Huang Y, Lei QH (2021) A generalized joint pyramid method for removability analysis of rock blocks: theoretical formulation and numerical implementation. Comput Geotech 132:103972

Wu J, Zhang ZX, Kwok CY (2015) Stability analysis of rock blocks around a cross-harbor tunnel using the improved morphological visualization method. Eng Geol 187:10–31

Wu W, Zhuang XY, Zhu HH, Liu X, Ma GW (2017) Centroid sliding pyramid method for removability and stability analysis of fractured hard rock. Acta Geotech 12(3):627–644

Yenier E, Sandikkaya MA, Akkar S (2010) Fundamental features of the extended strong-motion databank prepared for the SHARE Project, Deliverable D4.1-updated strong-ground motion. http://www.share-eu.org/sites/default/files/D4%201_SHARE.pdf. (**Accessed 12 Jun 2021**)

Yu QC, Ohnishi Y, Xue GF, Chen DJ (2009) A generalized procedure to identify three-dimensional rock blocks around complex excavations. Int J Numer Anal Meth Geomech 33:355–375

Zafarani H, Jafarian Y, Eskandarinejad A, Lashgari A, Haji-Saraei AE (2020) Seismic hazard analysis and local site effect of the 2017 Mw 7.3 Sarpol-e Zahab, Iran, earthquake. Nat Hazards 103:1783–1805

Zhang YB (2018) Earthquake-induced landslides: Initiation and run-out analysis by considering vertical seismic loading, tension failure and the trampoline effect. Springer, Berlin

Zhang ZX, Kulatilake PHSW (2003) A new stereo-analytical method for determination of removal blocks in discontinuous rock masses. Int J Numer Anal Meth Geomech 27(10):791–811

Zhang ZX, Lei QH (2013) Object-oriented modeling for three-dimensional multi-block systems. Comput Geotech 48:208–227

Zhang ZX, Lei QH (2014) A morphological visualization method for removability analysis of blocks in discontinuous rock masses. Rock Mech Rock Eng 47(4):1237–1254

Zhang QH, Wu AQ, Zhang LJ (2014) Statistical analysis of stochastic blocks and its application to rock support. Tunn Undergr Space Technol 43:426–439

Zhang ZX, Wang SF, Huang X, Kwok CY (2017a) TBM-block interaction during TBM tunneling in rock masses: block classification and identification. Int J Geomech 17:E40160015SI

Zhang ZX, Wu J, Huang X (2017b) Application of a vertex chain operation algorithm on topological analysis of three-dimensional fractured rock masses. Front Struct Civil Eng 11:187–208

Zhang ZX, Wang SF, Huang X (2018) Analysis on the evolution of rock block behavior during TBM tunneling considering the TBM-block interaction. Rock Mech Rock Eng 51(7):2237–2263

Zhang ZX, Wang SF, Huang X, Rostami J (2019) Application of block theory for evaluating face stability under disc cutters loading of TBM, case study of a water-conveyance tunnel project. Tunn Undergr Space Technol 90:249–263

Zhang LL, Sherizadeh T, Zhang YW, Sunkpal M, Liu HJ, Yu QC (2020) Stability analysis of three-dimensional rock blocks based on general block method. Comput Geotech 124:103621

Zheng J, Kulatilake PHSW, Shu B, Sherizadeh T, Deng JH (2014) Probabilistic block theory analysis for a rock slope at an open pit mine in USA. Comput Geotech 61:254–265

Zheng J, Kulatilake PHSW, Deng JH (2015a) Development of a probabilistic block theory analysis procedure and its application to a rock slope at a hydropower station in China. Eng Geol 188:110–125

Zheng YH, Xia L, Yu QC (2015b) A method for identifying three-dimensional rock blocks formed by curved fractures. Comput Geotech 65:1–11

Zheng YH, Xia L, Yu QC (2016) Analysis of removability and stability of rock blocks by considering the rock bridge effect. Can Geotech J 53:384–395

Zheng YH, Xia L, Yu QC (2019) Stability analysis method for rock blocks formed by curved fractures. Tunn Undergr Space Technol 85:182–195